International Journal of Nanoelectronics and Materials
IJNeaM
ISSN 1985-5761 | E-ISSN 2232-1535

Electrospun cellulose acetate/alginate incorporated with kaempferol enhances cells' proliferation activity in a hyperglycaemic microenvironment

Mira Aqilah Tajuddin[a], Siti Pauliena Mohd Bohari[ab]*, Aryanny Nasir[a] and Nurrulhidayah Salamun[a]

[a] *Faculty of Science, Universiti Teknologi Malaysia, 81310 Skudai, Johor, Malaysia*
[b] *Institute of Bioproduct Development, Universiti Teknologi Malaysia, 81310 Skudai, Johor, Malaysia*
∗*Corresponding author. E-mail: pauliena@utm.my*

Received 4 March 2025, Revised 13 August 2025, Accepted 29 October 2025

ABSTRACT

The treatment of diabetic wounds remains a global challenge, as their nature of delayed healing, which is due to the oxidative stress, persistent infection, and frequent dressing changes during the healing process, could risk limb amputations and even fatality. A variety of approaches have been undertaken to generate skin substitutes, wound-healing patches, or dressings with adequate barrier properties, degradation, exudate uptake capacity, and wound-healing capacity. This study aimed to evaluate a novel bioactive wound dressing from rice husk cellulose acetate (CA) electrospun loaded with kaempferol (KM) and layered with alginate solution (CA-KM/ALG) with the ability to deliver KM to the wound site. KM is highly enriched with multiple therapeutic agents that can promote cellular response and wound healing. In this study, electrospun CA nanofibers containing KM were first fabricated by the electrospinning method and then combined with the alginate hydrogel (ALG). The scanning electron microscopy images and macroscopic images revealed that CA nanofibers were fully covered with alginate hydrogel. FTIR results showed the successful incorporation of KM in nanofibers. Water contact angle, porosity, water uptake, and weight loss study of CA-KM/ALG (0°, 91.30 ± 4.72%, 600-650%, 50%). Fibroblast culturing on the fabricated dressings in both normal and hyperglycemic conditions demonstrated that cellular attachment and proliferation improved with suitable KM concentration (15.67 µg/mL). Taken together, our results provide a novel bioactive dressing with great potential for speeding up the healing process in severe wounds.

Keywords: *Time-frequency analysis, Failure diagnosis, Diagnostics in rotating machinery, Vibration analysis*

1. INTRODUCTION

Delayed healing of infected wounds is becoming more common over the years, which leads to compromising major part of management costs and mortality rates. These chronic wound infections and related consequences will continue to plague as long as the underlying causes, such as the development of diabetic wounds continue (Sen, 2021). On that note, wound treatment was observed to be revolutionized in the last few years, as it has been confirmed that moist dressings could accelerate wounds' healing and closure (Colobatiu et al., 2019). Theoretically, wound healing properties such as antimicrobial, biocompatibility, and non-toxicity would make the wound dressing an ideal choice, on top of being able to permit gaseous exchange and eliminate excess exudates, having appropriate mechanical properties, being easily removed without causing stress, and having a proper moisture balance (Nguyen et al., 2019). However, due to this ideal characteristic, which is still far from realisation, has been much research in innovating wound dressing. Coincidentally, there has been remarkable attention in the creation of bioactive wound dressings from polymers that can act as a carrier to deliver active substances or drugs to accelerate wound healing (Colobatiu et al., 2019).

Natural polymers such as cellulose can be obtained and extracted from plants such as sugarcane, cotton, and paddy rice (Gupta et al., 2018). Instead of only exploiting the plant itself, many researchers have been working on utilising their waste, such as rice husk, to convert them to wealth by creating valuable applications in various fields (Cheah et al., 2016). Rice husk (RH) is abundantly produced waste from rice mills and is reported to have contributed to a lot of agricultural waste management issues, but interestingly it comprises a substantial amount of cellulose (Gupta et al., 2018). RH cellulose has various interesting properties, such as low density and nonabrasiveness with reasonable strength and stiffness, apart from being a renewable natural polymer. Cellulose-based materials bear valuable qualities like biocompatibility and antioxidant properties, reported to be applied in controlling wound and organ transplants (Doostmohammadi et al., 2020). Not only that, cellulose derivatives such as methyl cellulose and cellulose acetate have been used for drug delivery because of their capacity to attach with bioactive substances (Doostmohammadi et al., 2020). Additionally, wound dressing made from cellulose and its derivatives can be manipulated into various forms, namely foam, hydrogels, and nanofiber scaffolds.

Nanofiber scaffolds have been fabricated using electrospinning technique and remarkably become the interest of research in a wide range of fields since the past decades due to their desirable characteristics (Kharaghani et al., 2018). The efficient method used which is electrospinning, enables the fabrication of ultrafine fibers with relatively high surface to volume ratio and high porosity. As a result, electrospun nanofibers have garnered considerable attention for various applications, particularly in the biomedical field. It has been reported that electrospun nanofibers are used as scaffolds for tissue engineering, membranes for delivering bioactive agents, and wound dressing materials (Liu et al., 2019). In this study, cellulose acetate (CA) was selected due to its proven biocompatibility and was electrospun as carrier for the delivery of bioactive agent (Wsoo et al., 2020). Electrospun CA fibers are widely used as drug carriers because of their excellent tissue compatibility and ease of fabrication (Wsoo et al., 2020). Various studies have also explored the incorporation of multiple compounds into nanofibers including antioxidant and anti-inflammatory agents such as flavonoids into electrospun CA fibers (Stoyanova et al., 2022).

Flavonoids hold interesting wound healing properties such that its antibacterial activity is linked to the suppression of bacterial energy metabolism and cytoplasmic membrane activity (Ullah et al., 2020). Kaempferol (KM) is a flavanol that also belongs to the class of flavonoids. It can be categorized as a phytonutrient, which plants naturally produce and has anti-inflammatory, antibacterial, and antioxidant functions (Yoon et al., 2013; Ren et al., 2019). But, even with numerous healing properties, KM has not been recorded to be applied as part of the wound dressing for treating cutaneous wounds. Even so, it appears to be that KM is a highly effective component that could be added and incorporated within wound dressings as a bioactive agent to encourage cell response and wound healing, particularly for the chronic wound group (Özay et al., 2019).

Electrospun CA are extensively used as drug carriers and were used in this study to incorporate KM, as it offers a unique avenue for other flavonoid delivery while providing a matrix for wound regeneration due to their flat geometry (Ullah et al., 2020). However, although electrospun nanofibers have made great progress as a type of multifunctional biomaterial, major challenges still remain to fully meet the needs of patients in terms of biodegradation control rates, drug release, and cell adhesion properties to mimic the natural wound healing processes (Memic et al., 2019). To address this issue, this study has added another natural polymer, which is alginate hydrogel, on top of the electrospun CA. Hydrogels are widely used in pharmaceutical industries, including wound dressings and controlled drug release, and own desirable properties in wound healing, such as being nontoxic, biodegradable, and better at cell adhesion, making them a perfect addition to fabricate an ideal wound dressing (Tran et al., 2020).

2. MATERIALS AND METHODS

2.1. Materials

The materials used in this study are as followed: cellulose acetate extracted from rice husk, sodium alginate (Sigma-Aldrich), acetone (Ac) (99.5%) (Sigma-Aldrich), ethanol (EtOH) (99.5%) (Sigma-Aldrich), N,N-dimethylacetamide (DMAc) (99%) (Sigma-Aldrich), kaempferol (K0133- 100 mg, 90% HPLC) (Sigma-Aldrich), human dermal fibroblast cell line (HSF, C-013-5C, at passage number 11), (TE Lab, UTM), 4.5 g/L Dulbecco's Modified Eagle Medium (DMEM), both with and without sodium pyruvate (for samples with alginate hydrogel) (DMEM-HPSTA), (Capricorn Scientific), fetal bovine serum (FBS, product code: FBS-11A) (Capricorn Scientific), sterile-filtered phosphate buffer saline solution (PBS, Item code: 806552-1L) (Merck), trypsin-EDTA solution (0.25%, sterile-filtered, BioReagent, Item code: T4049) ((Sigma Aldrich), trypan blue solution (0.4%, liquid, Item code: T8154) (Sigma Aldrich), antibiotic-antimycotic (100 x), Catalog number:15240062 (Thermo Fisher Scientific), MTT powder (Sigma Aldrich), and cell counting kit (CCK-8) (500 test) (Enzo).

2.2. Process Flow

Figure 1 depicts a process flow of establishing electrospun cellulose acetate loaded with KM and layered with alginate solution as a diabetic wound dressing.

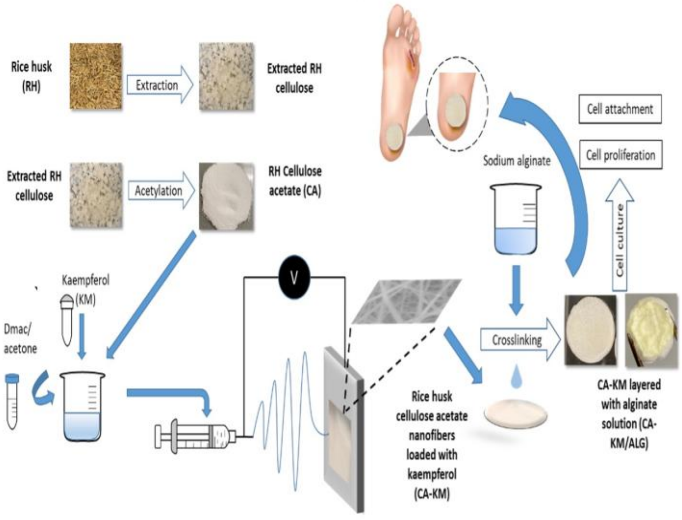

Figure 1. Process flow of establishing electrospun cellulose acetate-kaempferol/alginate nanofibers mat for chronic wound application.

2.3. Source of Plant Materials

The Oryza Sativa L. husk was purchased from a local paddy supplier, En. Basir Mohd Piah, in Alor Setar, Kedah, in November 2019. This plant sample was then sent for species identification and was authenticated by Dr. Sam Yen Yen at Forest Research Institute Malaysia (FRIM), Kepong. The sample was deposited with voucher specimen number PID 010122-01 in the Herbarium of FRIM.

2.4. Cellulose Extraction from Rice Husk (RH)

The cellulose extraction from RH was carried out according to the method by Rbihi et al. with slight modification. RH sample was cleaned, filtered, and oven-dried overnight at 80 ℃. The extraction process began by mixing a 10 g of RH with a toluene:ethanol mixture (2:1) using a magnetic stirrer for 6 hours to remove the pigments and lipids, followed by oven drying at 80 ℃ overnight (Sankararamakrishnan et al., 2019). The RH was then treated with 4% of sodium hydroxide (NaOH) for 4 hours at 80 ℃ to remove part of the hemicellulose (Rbihi et al., 2019). The suspension was filtered and washed with distilled water (dH_2O) until it reached pH 6-7. This was followed by bleaching treatment using 1.4% sodium chlorite ($NaClO_2$) and 10% acetic acid at 80 ℃, which facilitates the degradation of lignin. The process was then followed by alkaline treatment with 0.1 M NaOH after which the suspension was rinsed with dH_2O until it reached pH 6-7 and was oven-dried overnight at 50 ℃ (Sankararamakrishnan et al., 2019).

2.5. Instrumentation Analysis to Characterize RH Cellulose

2.5.1. Characterization of RH Samples by Fourier Transform-Infrared Spectroscopy (FTIR)

The FTIR analysis by FTIR spectrometer Perkin Elmer Model Frontier (T05, UTM) was performed to measure the infrared spectrum emission of the extracted RH cellulose. Three samples of RH cellulose (raw, treated with alkali, and after-bleached RH) were analysed to identify the changes in samples' functional groups after consecutive treatments and to confirm the treatment success by observing the samples' chemical properties (Onoja et al., 2019). Before the acquisition of each spectrum of the sample, the attenuated total reflectance (ATR) plate and probe were wiped using 75% ethanol. Then the samples were placed on the plate and pressed against a high refractive index prism. FTIR spectrometry analysis was measured at 4 cm^{-1} resolution and the spectral scanning wavelength within the range of 400-4000 cm^{-1} (Kruer-Zerhusen et al., 2018).

2.5.2. Characterization of RH Samples by Scanning Electron Microscope (SEM)

The macroscopic observation of treated RH cellulose samples was examined under a scanning electron microscope (SEM, Hitachi TM3030). Prior to imaging, the samples were fixed onto metal stubs using double-sided conductive tape and vacuum-coated with a 12 nm layer of gold for 15 minutes. The scanning was performed at an accelerating voltage of 15 kV to enhance image quality by reducing surface charging (Ali et al., 2014; Wang et al., 2018).

2.5.3. Acetylation of RH Cellulose

The extracted RH cellulose was synthesized and transformed into its derivate, cellulose acetate (CA) by acetylation. For the initial process of cellulose acetylation, which was performed inside the fume hood, extracted RH cellulose weighing 2.5 g, was added into glacial acetic acid and was heated on a hot plate for 1 hour at 47.5 ℃. The mixture was constantly stirred with the use of a magnetic stirrer under the same condition (Das et al., 2014; Wang et al., 2020). Subsequently, acetic anhydride in the amount of 5 mL was dropped into the mixture along with a few drops of 5.5 v/v % sulphuric acid (approximately 1 mL) as a catalyst to replace the -OH group of cellulose with an acetyl group. The slurry was continued to be heated on a hot plate at 47.5 ℃ for 2 hours (Achtel & Heinze, 2016).

2.6. Instrumentation Analysis to Characterize RH Cellulose Acetate (CA)

2.6.1. RH CA Characterization by FTIR

The FTIR analysis by FTIR spectrometer Perkin Elmer Model Frontier (T05, UTM) was run to observe the peak intensity and measure the infrared spectrum emission of the RH CA sample and to analyze the replacement of functional groups of the polymers (Onoja et al., 2019). The FTIR analysis of RH CA was conducted using the same protocol as for raw and treated RH samples, involving ATR mode at a resolution of 4 cm^{-1} and a scanning range of 400-4000 cm^{-1}.

2.6.2. Scanning Electron Microscope (SEM)

The SEM characterization of RH CA followed the same protocol used for RH samples, where samples were fixed onto metal stubs and coated with gold prior to imaging under a Hitachi TM3030 microscope (Ali et al., 2014; Wang et al., 2018).

2.7. Electrospinning Technique

2.7.1. Preparation of Polymer Solutions

RH CA-KM solutions at concentrations 15% and 17% were prepared by incorporating kaempferol (KM) at a concentration of 15.67 ug/mL (Özay et al., 2019). The solution was continuously and vigorously stirred using a magnetic stirrer for 4 hours at 25 ℃ until a homogeneous solution was formed (Huan et al., 2015; Pinheiro Bruni et al, 2020).

2.7.2. Electrospinning Setup

The electrospinning process of the CA solution began by connecting 10 mL plastic syringes fitted with blunt-ended metal needles (0.84 mm). Aluminium foil was positioned on a wooden stand to collect the blended solutions, while a high voltage power supply generated a positive DC voltage of 12 kV (Konwarh et al., 2013; Long et al., 2019). The blended sample solutions were then loaded into the syringes and manually pushed until the solution reached the needle tip, at which point the electrospinning was initiated. The distance between the needle tip and collector was maintained at 14 cm throughout the experiment. The flow rate of the solutions was kept constant at the rate of 1

mL/hour. The electrospinning experiment was carried out at room temperature (Kalita et al., 2015; Long et al., 2019).

2.8. Characterization of the Prepared Electrospun Nanofibers

2.8.1. Scanning Electron Microscopy

The surface morphology of CA and CA-KM, CA/ALG and CA-KM/ALG nanofibers was examined using a scanning electron microscope (SEM), following the procedure described for RH samples, where samples were fixed onto metal stubs and coated with gold prior to imaging under a Hitachi TM3030 microscope (Ali et al., 2014; Wang et al., 2018).

2.8.2. Contact-angle Measurement

The surface wettability of the samples (CA, CA-KM, CA/ALG, CA-KM/ALG) was obtained by using a fixed, immobile drop of the contact angle system (VCA Optima, AST Products, Inc.). A water droplet of 0.5 µl was fixed on the membrane surface of the samples (Huhtamäki, 2018). A real-time high-resolution camera captured the image of the droplet, and the contact angle was analysed by using the ImageJ software. The ImageJ plug-in was used to calculate the contact angle of a water droplet on the samples' surface using the approximation of the sphere and ellipse. The test was repeated three times to take the average result (Lamour et al, 2010; Huhtamäki, 2018).

2.8.3. Alginate Solution Preparation

1.5 g of sodium alginate was properly mixed in deionized water at a final concentration of 1.5% (w/v) in a 250 mL Erlenmeyer flask using a magnetic stirrer (Jang et al., 2014; Shelke et al., 2016). The mixing was continued for 1 hour to obtain low molecular weight (LMW) sodium alginate (Shelke et al., 2016).

2.8.4. Layering Alginate Solution on Electrospun Nanofiber Mats

The electrospun nanofiber mat was cut into circular discs with an area of approximately 1 cm^2, and 1.5% (w/v) sodium alginate solution was added to the nanofiber mat and allowed to sit for 10 minutes. The sample was placed for 1 hour at room temperature to allow sodium alginate to gel on top of the mat and promote uniform sodium alginate layers. These discs were then added with 0.1 M calcium chloride solution to cross-link the sodium alginate solution for 15 minutes. The discs with sodium alginate and calcium chloride solution were left in the incubator shaking at 4 °C to form the hydrogel layer (Zhijiang et al., 2018).

2.9. Characterization of Rice Husk Cellulose Acetate Loaded with Kaempferol by Electrospinning Process and Layered with Alginate (CA-KM/ALG)

2.9.1. Porosity study

The porosity of the samples (CA, CA-KM, CA/ALG, and CA-KM/ALG) was measured according to Equation 1 (Razak et al., 2016). V_d is the volume of the samples and was determined by measuring the volume of the absorbed cyclohexane. While V_p is the pore volume, determined by immersing the samples in cyclohexane with the density of 0.778 g/cm^3 (Razak et al., 2016).

Porosity: $V_p/(V_d+V_p)$ x 100 (1)

2.9.2. Water Uptake Behaviour Study

The water uptake behaviour of the samples (CA, CA-KM, CA/ALG, and CA-KM/ALG) was evaluated by weighing the samples (W_0) prior to immersing them in a wound-like solution (Xie et al., 2021). The samples were cut into a size of 1 cm × 1 cm ×1 cm respectively, and the initial weight was recorded. The samples were then immersed in the wound-like solution and proceeded to be incubated overnight at 25 °C. The samples were taken out and slightly dried using filter paper every 48 hours for 15 days (W_1) (Ravikumar et al., 2017). Equation 2 is for the calculation of the samples' water update and was identified as the water uptake rate (%) (Yousefi et al., 2018).

Water Uptake (%): $((W_1-W_0)/W_0) \times 100$ (2)

2.9.3. Weight Loss Study

The weight loss study of the samples (CA, CA-KM, CA/ALG, and CA-KM/ALG) was analysed by calculating the weight loss of the samples after freeze-drying (Xie et al., 2021). The samples immersed in the wound-like solution were weighed to get the initial reading (W_1). Then, the samples were freeze-dried in a freeze dryer at -50 ºC every 48 hours for 15 days and weighed (W_0) until a constant weight was achieved (Ambekar et al., 2019). The weight loss rate was calculated by using equation (3) (Adeli et al., 2019).

Weight Loss (%): $((W_0-W_1)/W_1) \times 100$ (3)

2.10. Bioassay Testing

2.10.1. MTT Assay

For the cytotoxicity study, tetrazolium reduction assay (MTT) was used (Latif et al., 2019). The Human Skin Fibroblast (HSF) cells were grown to confluency and then trypsinized using 1 mL of 0.25% to detach the cells. The pre-prepared cells were seeded onto the mat at a cell density of approximately 5×10^4 cells/well in DMEM under normoglycemic culture conditiond (25 mM of glucose concentration) and hyperglycemic culture conditions (150 mM of glucose concentration), respectively, and incubated at 37 °C in 5% CO_2 (Wiegand et al., 2019). Different concentrations of KM were then added to a 96-well plate containing HSF cells under normoglycemic and hyperglycemic microenvironments. Serial dilutions ranging from 1000 µg/mL to a final concentration of 7.8

μg/mL were tested (Latif et al., 2019). Next, 20 μL of MTT reagent was prepared by dissolving MTT powder in PBS. The solution was then filter-sterilized using a syringe-driven filter (0.20 μm pore size) into a wrapped Falcon tube to obtain a homogenous solution and remove any undissolved particles (Wiegand et al., 2019). Next, the MTT solution was added to the well after 72 hours of incubation of the mat with HSF. The mat was incubated for 4 hours prior to the addition of 100 μL of 0.1 M HCl/isopropanol solution for 15 minutes. Then, 150 μL of the resulting colored solution was added (Chang et al., 2012; Latif et al, 2019). Upon solubilization of the formazan crystals, the absorbance (Abs) was measured using the enzyme-linked immunosorbent assay (ELISA) reader (SPECTRO star Nano, Germany) at a wavelength of 570 nm to evaluate cell viability (Latif et al., 2019). Equation (4) was used to calculate cell viability:

Cell viability (%): (Abs sample-blank)/(Abs control-blank) x 100 (4)

2.10.2. Cell Attachment Assay

Samples of CA, CA-KM, CA/ALG, and CA-KM/ALG were cut into 1 cm^2 pieces for CA and CA-KM nanofibers and 1 cm^3 pieces for CA/ALG and CA-KM/ALG samples and sterilized under UV light. The samples were then rinsed with prepared phosphate buffered saline (PBS, pH 7.0), and transferred into a 24-well plate containing culture medium, followed by overnight incubation in a humidified CO_2 incubator at 37 ℃ prior to cell seeding. Fibroblast cells (HSF1180) were cultured under both normoglycemic and hyperglygemic conditions in Dulbecco's Modified Eagle Medium (DMEM) supplemented with 10% fetal bovine serum (FBS) and 1% penicillin-streptomycin in a 5% CO_2 atmosphere at 37 ℃. The medium was then removed from 24-well plate, and each well was seeded with 500 μL of cell suspension at a density of 5×10^4 cells/well to allow attachment on the surface of samples (CA, CA-KM, CA/ALG, and CA-KM/ALG). The cells were incubated for 4 hours in CO_2 incubator (5% CO_2, 37 ℃). After incubation, 50 μL of CCK-8 solution was added to each well containing samples, and the plates were further incubated for 2 hours at 37 ℃ in a CO_2 incubator. The absorbance of each well plate was measured at 450 nm using an ELISA microplate reader (Rezk et al., 2019).

2.10.3. Cell Proliferation Assay

Samples of CA, CA-KM, CA/ALG, and CA-KM/ALG were cut with the measurement of 1 cm^2 for CA and CA-KM nanofibers and 1 cm^3 for CA/ALG and CA-KM/ALG samples and sterilized under UV light. The samples were then rinsed with prepared phosphate buffered saline with pH 7 three times and then were transferred to a 24-well plate containing culture medium and incubated overnight in a humidified atmosphere at 37 ℃ prior to cell seeding. The fibroblast cells (HSF1180) were cultured in normoglycemic and hyperglycemic environments (DMEM medium, complemented with 10% fetal bovine serum (FBS) and 1% penicillin-streptomycin in the condition of 5% CO_2 at 37 ℃). The medium was removed from 24-well plate and the plate was seeded with 500 μL of 5×10^4 cells/well to attach on the surface of the samples (CA, CA-KM, CA/ALG, and CA-KM/ALG) and grown at different hours (24, 48, and 72 hours) in atmosphere of 5% CO_2 at 37 ℃. The plate was incubated for 4 hours, and 50 μL of CCK-8 solution was poured into the well containing samples. The plate was continued to be incubated for 2 hours in a CO_2 incubator at 37 ℃. 100 uL culture from each well was transferred to a 96-well plate. The absorbance of each well plate was evaluated at a wavelength of 450 nm using an ELISA microplate reader (Rezk et al., 2019).

2.10.4. Statistical Analysis

All data were represented as the means ± SD of the results of experiments with different nanofiber samples, and all data were analyzed using SPSS-V25 software. Statistical analyses were performed by comparing the means of the two groups' values using the Student's t-test or Mann–Whitney U test where appropriate. P-values of $p<0.01$ and $p<0.05$ were referred to determine significant differences.

3. RESULT AND DISCUSSION

3.1. Cellulose and Cellulose Acetate from Rice Husk (RH)

The optical photos of the rice husk sample that was chemically treated in a series of stages: raw, alkali-treated, bleached, and acetylated, are shown in Figures 2a-2d. It was observed that the raw rice husk colour started to change from yellowish (chemical treatment) in Figure 2a to brownish (alkali treatment) in Figure 2b and whitish (bleaching) in Figure 2c. This result may be attributed to the chemical treatment efficiency in purifying the cellulose fibers and removing the non-cellulosic components of RH as reported by previous research (Onoja et al., 2019). After the bleaching treatment with sodium chlorite ($NaClO_2$), the colour changes of the samples were more apparent. The cellulose microfibrils also turned almost white in colour, as shown in Figure 2c. This result proved the successful removal of the non-cellulosic components and agrees with those reported by previous researchers (Paschoal et al., 2015; Ilangovan et al., 2020). Typically, a mixture of sodium chlorite (70%) and acetic acid (80%) is used to successfully remove the chemical components of lignin, hemicelluloses, and other significant lignocellulosic debris from plant-based fibers (Maver et al., 2020). A study where two banana cultivars have also had their cellulose isolated and their lignin extracted using a similar acid mixture, doing away with the non-cellulose polysaccharides and the traditional delignification and bleaching procedure in the process (Gopinath et al., 2018). This can be explained in further characterisations of ATR-FTIR as presented in Figure 4 and SEM images in Figure 5.

Error! Reference source not found.d shows an image of acetylated cellulose from rice husk. The texture was powdery and became off-white in colour after the filtration phase. The acetylation mechanism can be classified as a heterogeneous process. When the sulphuric acid (H_2SO_4) was added, the carbonyl carbon of the acetic anhydride was

activated. This is possible due to the presence of an alcoholic group (Krishnadev et al., 2020). After the activation, acetic anhydride would react with cellulose hydroxyl groups and the esterification would take place, resulting in the production of acetic acid as a by-product (Das et al., 2014; Araujo et al., 2020). In contrast, the typical process of acetylation occurs as a homogeneous process by having sulphuric acid (H_2SO_4) perform as a catalyst aiding to dissolve the cellulose extract in the acetic acid, the reaction medium. In this study, the process of heterogenous acetylation was performed via displacement of hydroxyl groups with acetyl groups by using acetic anhydride, following the method adopted from Araujo et al., (2020). The result can be observed in the characterisations shown in **Error! Reference source not found.** and **Error! Reference source not found.**.

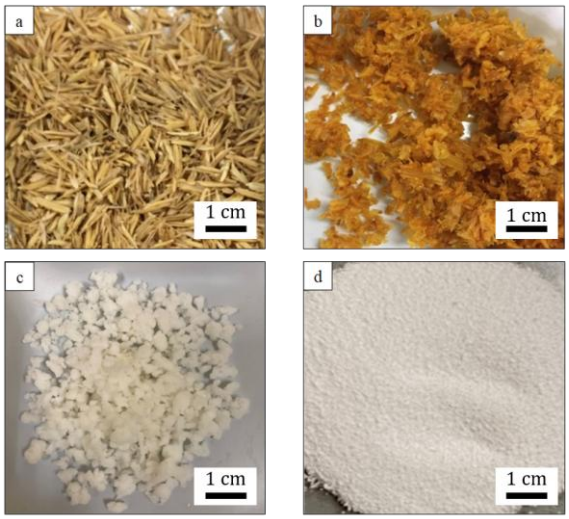

Figure 2. Images of (a) raw rice husks (RH) sample, (b) alkali-treated RH sample, (c) bleached RH sample, and (d) cellulose acetate RH sample. Each image includes a scale bar representing 1 cm for visual reference.

The reversible reaction in the acetylation of cellulose acetate from RH cellulose can be visualized in Figure 3. When observed, parts of OH groups in cellulose were replaced by the acetyl group in cellulose acetate by the source of esters, acetic anhydride. Highly acetylated cellulose is formed when most of the OH groups in the cellulose structure are replaced by acetyl groups during acetylation (Tian et al., 2021). This contributes to a higher degree of substitution (DS) in cellulose acetate. The degree of substitution ranging from ~0.8 to 3.0 defines the level of hydrophobicity properties in cellulose acetate (Suwantong et al., 2010; Alves et al., 2019). Normally, CA with a degree of substitution that is equivalent to 1.0-1.5, 2.0-2.5, and 2.75-3.0 is typically referred to as monoacetate, diacetate, and triacetate cellulose, respectively (Wsoo et al., 2020). In this study, however, the DS was not determined and the chemical interactions as well as hydrophobicity were further investigated using ATR-FTIR characterisation and a water contact angle study instead. Although the DS was not quantitatively determined in this study, the successful acetylation of cellulose was confirmed through ATR-FTIR analysis. The peaks corresponding to ester carbonyl groups (C=O) and reducing hydroxyl stretching intensity (–OH) indicated the replacement of hydroxyl groups with acetyl groups. Additionally, changes in water contact angle measurements supported the increased hydrophobicity of the acetylated cellulose, indirectly reflecting a successful substitution process.

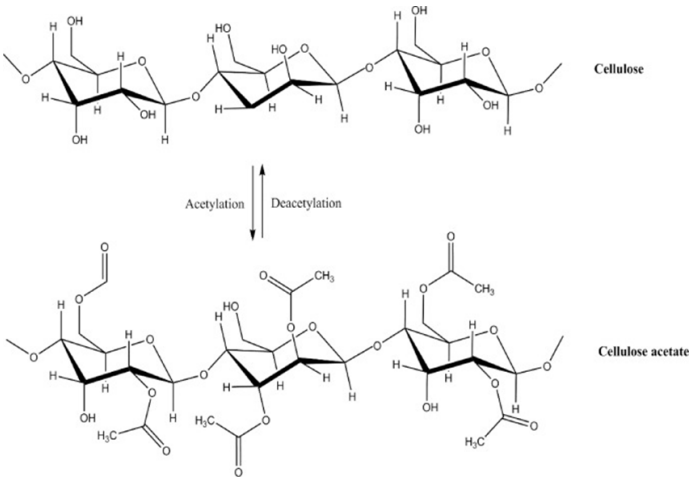

Figure 3. Chemical structure of RH cellulose and cellulose acetate RH in the reversible reaction.

3.2. Morphological and Chemical Characterizations of RH Cellulose and Cellulose Acetate

3.2.1. Chemical Interaction Analysis by Fourier-Transform Infrared Spectroscopy (FTIR)

To prove the successful acetylation of cellulose from RH, the comparison in FTIR spectra of RH CA with other extracted RH samples is visualized in Figure 4 (a-d). The figure shows a comparative FTIR spectrum between raw RH, alkali-treated RH, bleached RH cellulose, and cellulose acetate RH, respectively. FTIR analysis is an insightful technique to distinguish between various samples by referring to their chemical components (functional groups) and to understand the characteristics of materials (Kurečič et al., 2018). In Figure 4, based on the dashed lines that indicate peaks and functional groups, it is recorded and circled in red that near the peak 3260-3328 cm^{-1}, all spectra showed a vibration band that corresponds to O–H stretching vibration for the intramolecular H-bond. However, in the CA spectrum in Figure 4 (d), the peak has shifted further to 3464 cm^{-1}. This hydrophilic tendency is reflected by the broad absorption band region related to the –CH and –OH groups of cellulose, present as their main components. The twin peaks in all spectra at 2852 and 2920 cm^{-1} in the middle area indicate the cellulose polysaccharides of aliphatic saturated C–H stretching vibration (Hasanvand et al., 2018). A significant individual peak at 1745 cm^{-1} is responsible to the stretching vibrations of the carbonyl functional group (C=O) of the acetyl ester group in the CA (Wsoo et al., 2021). The peaks located around 1628-1635 in all spectra are the O-H bond of water absorption (Jatoi et al., 2019). A shift in the C-H group's symmetry can be seen in the peak at roughly 1370 cm^{-1} in the spectra of the treated RH sample (Johar et al., 2012; Kalwar et al., 2018). The bands around 980-1036 cm−1 seen in all four of the spectra relate to the structure of the cellulose compositions as well

as the C-H stretching vibration of C-O (Kalwar et al., 2018). While the minor signature at 844, 866, and 903 cm^{-1} in alkaline-treated, bleached, and acetylated cellulose, as shown in Figure 4, shows the common cellulose structure, attributed to the β-glycosidic chain of the glucose ring of cellulose. At the peak of 794 cm^{-1} in raw RH, it represents the hemicelluloses' uronic ester groups comprised. Additionally, the peak corresponds to the ferulic and p-coumeric acids in lignin and hemicellulose content, which is the ester chain of the carboxylic group. The peak dissolved following RH chemical treatment, determining that the non-cellulosic components have been removed (Johar et al., 2012; Kalwar et al., 2018). The prominent peaks are reported and simplified in Table 1.

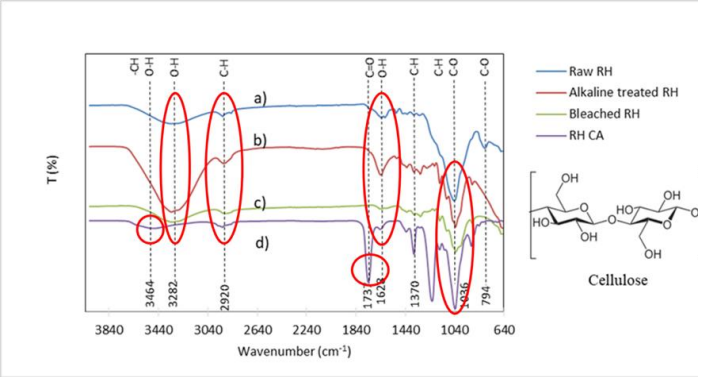

Figure 4. FTIR spectra recorded for (a) raw rice husk (Raw RH), (b) alkaline treated rice husk (alkaline treated RH), (c) bleached rice husk (Bleached RH), and (d) rice husk cellulose acetate (RH CA)

Table 1 Peak absorption of rice husk at different treatment stages

Rice Husk (RH)				Involved Groups
Raw	Alkali treated	Bleached	CA	
3260-3412	3268-3328	3298	3464	O-H group strain
2852, 2920	2890	2916-2918	2920	C-H group strain
-	-	-	1737	C=O stretching vibration
1628	1628	1620	1635	O-H bond of water absorption
-	1370	1370	1370	C–CH_3
980	956	1099	1036	C–H stretching vibration, C–O and the cellulose constituent's structure
-	844	866	903	C-O stretch C-H vibration in cellulose
794	-	-	-	C-O bond in cellulose/hemicellulose /lignin

3.2.2. Microscopic Characterizations by SEM (Scanning Electron Microscope) of RH Cellulose and Cellulose Acetate

Following the macroscopic observations described in the previous section, microscopic observations were conducted using a scanning electron microscope (SEM) to visualize the morphological changes of the samples (Kurečič et al., 2018). However, due to the use of different magnifications for each sample, direct comparison between the samples is limited, and observations were instead made within individual micrographs and between samples captured at the same magnification to ensure consistency and validity in structural comparison. The SEM image of the untreated RH (Figure 5a) has been evidently well-organized with uneven outer structures due to the presence of silica, similar to those reported by previous researchers (Johar et al., 2012; Kalwar et al., 2018). As a result of partial elimination of lignin and hemicellulose, the raw RH has deformed after alkali treatment with NaOH (w/v) (Figure 5b). The structure appeared disorganized and less compact, indicating the partial removal of the cementing components indicated in Figure 5a. Such treatment has successfully eliminated the waxy components from the RH surface, as well as the pectin, lignin, and hemicellulose (Kurečič et al., 2018). In Figure 5c, the bleached RH fibers appeared more individualized and elongated compared to raw RH in Figure 5a and alkali-treated RH in Figure 5b. This morphological change indicates successful removal of non-cellulosic cementing materials such as lignin and hemicellulose during the bleaching process, suggesting a higher aspect ratio in the bleached RH. This fiber morphology is favourable for transformation into electrospun fiber due to improved spinnability and fiber continuity (Krishnadev et al., 2022). The acetylation process is known to derive cellulose fiber structure through esterification, potentially improving fiber separation (Sghaier et al. 2012; Fareez et al. 2018). In Figure 5d, the cellulose acetate (CA) fibers appeared to be more uniformly distributed with a relatively refined and organized morphology, suggesting that the acetylation process may have improved the fiber dispersion.

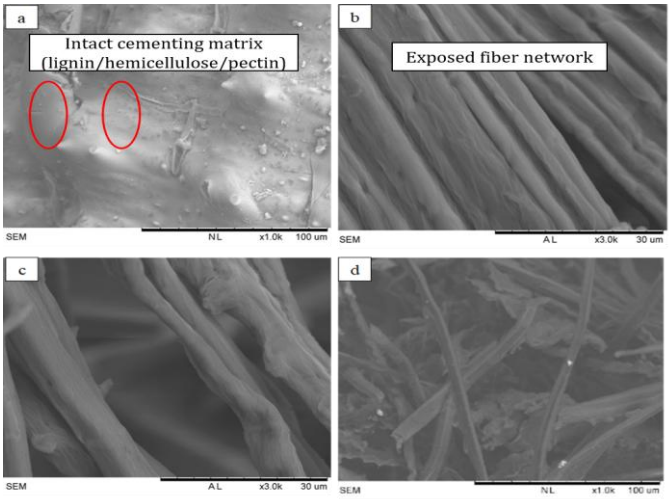

Figure 5. SEM images of (a) Raw RH at a magnification of 1000x, (b) Alkaline-treated RH (3000x) (c) Bleached RH (3000x), and (d) RH CA (1000x).

3.3. CA Nanofibers Loaded with Kaempferol (KM) Layered with Alginate Solution (CA-KM/ALG) Characterizations

3.3.1. Surface Morphological Characterization of CA Nanofibers

Morphological observations of electrospun cellulose acetate (CA) nanofibers at 15% and 17% (w/v) concentrations are shown in Figures 6a and 6b, respectively. The fibers produced from the 15% CA solution exhibited visible beads along the fibers, particularly concentrated near the center of the image (Figure 6a), indicating an unstable jet formation during electrospinning. In contrast, fibers produced from the 17% CA solution appeared smoother and bead-free (Figure 6b), suggesting more stable electrospinning conditions and improved fiber quality. These findings demonstrate that increasing CA concentration improved fiber uniformity and reduced bead formation in our system. This is likely due to the increased viscosity of the polymer solution at higher concentrations, which promotes continuous and stable jet flow during electrospinning. Our results are in agreement with Angel et al. (2020) and Nasir et al. (2023), who reported that higher CA concentrations tend to suppress bead formation and yield more consistent fiber structures. Furthermore, previous studies (e.g., Haas et al., cited in Mashfeghian et al., 2021) have established that a 2:1 acetone/DMAc solvent mixture effectively supports the electrospinning of CA solutions within the 12.5–20% range, which aligns with our optimized 17% formulation. Therefore, the main finding from Figure 6 is that 17% CA produced the most morphologically stable nanofibers in our experimental conditions, validating the selected polymer concentration for subsequent KM loading.

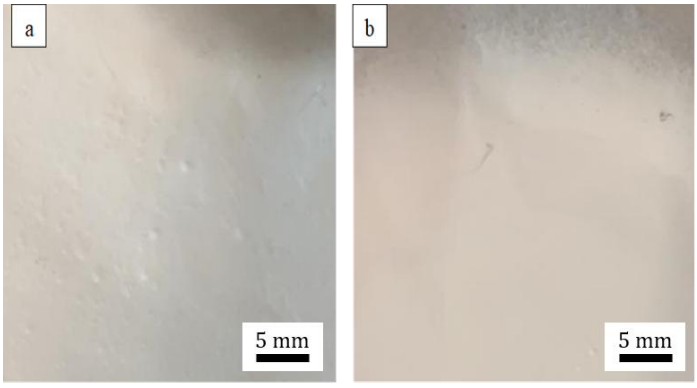

Figure 6. Images of (a) 15% CA nanofibers and (b) 17% CA nanofibers surface taken after the electrospinning process was completed

3.3.2. Surface Morphological Characterization CA Nanofibers Loaded with KM (CA-KM)

According to the comparison between 15% and 17% CA nanofibers in terms of morphology and wettability, 17% (Figure 6b) showed better fiber surface and distribution. Hence, kaempferol was dissolved in 17% CA polymer solutions for electrospinning to fabricate the CA-KM nanofibers. In Figure 7, both CA and CA-KM nanofibers were compared to see the nanofibers' surface structure. Both fiber surfaces showed a uniform fiber structure with little to no visible beads, and no significant morphological differences were observed.

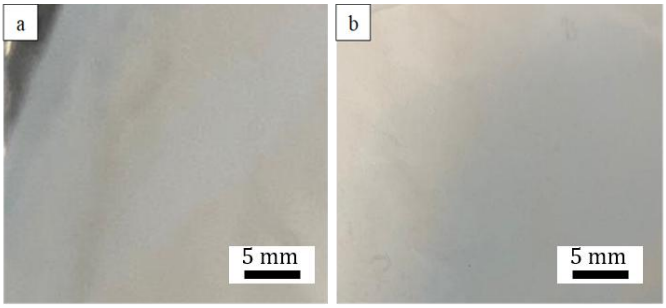

Figure 7. Images of (a) CA nanofibers surface (b) CA-KM nanofibers surface taken after the electrospinning process was completed

3.3.3. Surface Morphological Characterization of CA Layered with Alginate Solution (CA/ALG) and CA-KM/ALG

The morphology of the CA/ALG and CA-KM/ALG scaffolds was observed to have a sponge-like structure after being lyophilised, with pores apparent on the surface of both scaffolds and within the scaffolds' 3D structure (Zhang et al., 2020). In Figure 8a, the CA/ALG scaffold was virtually white, circular, and porous. Meanwhile, in Figure 8b, there were yellowish stains on the CA-KM/ALG shown, which was believed to be caused by KM being released from the CA-KM nanofiber during the layering of alginate hydrogel. The yellowish crystal powder with a melting point of 278 °C, KM, was dissolved in the electrospun CA solvent prior to electrospinning. The wrinkle obtained on the hydrogel on the CA-KM/ALG shown in Figure 8b might be attributed to the drying process compared to the rather flat hydrogel obtained from the CA/ALG shown in Figure 8a (Ye et al., 2019). This confirmation of KM loading success in the CA-KM nanofibers was further proven in ATR-FTIR characterisation in Figure 9.

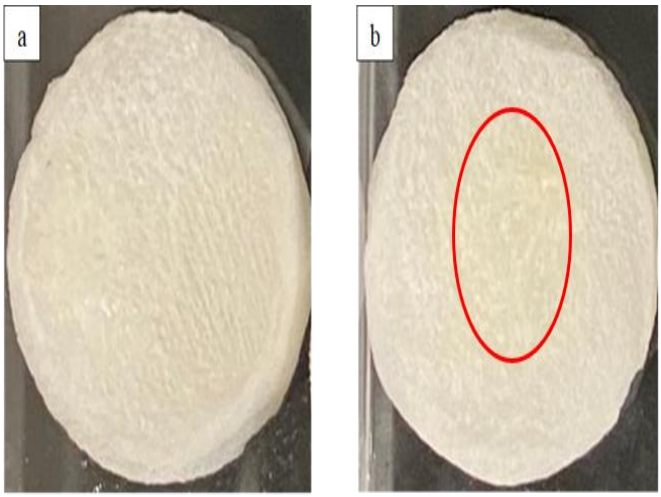

Figure 8. Images of (a) CA/ALG and (b) CA-KM/ALG from top view with a diameter of 2 cm

3.4. Morphological and Chemical Characterizations of CA-KM, CA/ALG, and CA-KM/ALG

3.4.1. Chemical Interaction Analysis by ATR-FTIR

To further confirm the incorporation of KM in the scaffold of CA nanofibers and CA-KM/ALG, the FTIR spectrum of CA derived from RH, KM, and CA-KM/ALG were compared in Figure 9 (a-e). The use of FTIR analysis is important to determine the characteristics of materials and to distinguish between different samples based on their chemical components (functional groups) (Kurečič et al., 2018). The main peaks are reported in Table 2. The successful incorporation of KM with CA nanofibers was proven by performing ATR-FTIR spectroscopy. Additionally, FTIR was able to depict the appearance of potential bonds that probably formed only after the incorporation. The spectra of electrospun CA nanofibers without KM (CA) and with KM (CA-KM) are shown in Figures 9a and 9c. Pure CA nanofibers' spectra showed cellulose acetate's distinctive bands, including a wide band at 3330-3505 cm^{-1} that is associated with the extended vibrations of the -OH group (Kurečič et al., 2018).

The absorbances around 2910 cm^{-1} and at 1370 cm^{-1} were probably due to the stretching and C–H bond vibration (Candido et al., 2016), respectively. The intense band at 1739 cm^{-1} was related to the extension of the C=O bond of the ester carbonyl group, while the sharp band at 1219 cm^{-1} aligned with the C–O bond vibration. The absorption peak at 1031 cm^{-1} was associated with the C–O–O vibration (Kurečič et al., 2018). This band absorption is typical for CA sp^2 hybridisation (O=C–O–CH_3) (Candido & Gonc¸alves 2016). In CA-KM nanofibers, a sharper peak or absorption band was observed at 2852 and 2918 cm^{-1}, which corresponded to –NH2 group scissoring vibrations. While the absorption peak at 1523 cm^{-1} was related to the benzene ring stretching that appears in the benzocaine structure (Kurečič et al., 2018).

The confirmation of successful KM incorporation into the CA nanofiber structure in Figure 9c can also be observed from the absorption peak at 774 cm^{-1}. For alginate hydrogel, the identification can be observed from the broad absorption band at 3298 cm^{-1}, corresponding to the -OH group in the hydrogel. In CA-KM/ALG in Figure 9e, the presence of KM can be denoted at sharper peaks at 2920 cm^{-1} and 2852 cm^{-1}, determining C-H group stretching. This is similar to the absorption bands annotated in CA-KM nanofibers spectra (Kurečič et al., 2018). These findings suggest successful chemical interaction between KM and CA, as well as stability of the drug within the polymer network. The detection of specific functional groups associated with KM and their persistence in the composite system highlight the potential of CA nanofibers and CA-KM/ALG hydrogels as effective drug delivery platforms.

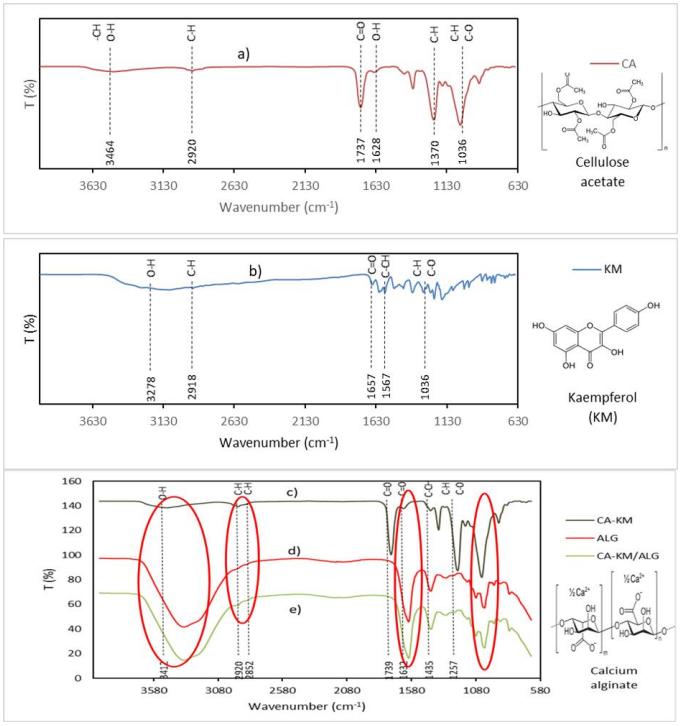

Figure 9. FTIR spectra recorded for (a) CA nanofibers, (b) kaempferol (KM), (c) CA-KM nanofibers, (d) alginate, and (e) CA-KM/ALG nanofibers.

Table 2. ATR-FTIR spectra of electrospun CA nanofibers with and without incorporated KM

CA-KM/ALG					Involved Groups
CA	CA-KM	ALG	CA-KM/ALG	KM	
3260-3412	3268-3328	3298	3472	3278	O-H group strain
2852, 2920	2890	2916-2918	2920	2852, 2918	C-H group strain
-	-	-	1739	1657	C=O stretching vibration
1628	1628	1620	1635	1608,	C=O absorption band
-	1370	1370	1370	1567, 1435	C–CH_3
980	956	1099	1036	1257	C–H stretching vibration of C–O and cellulose constituent's structure
-	844	866	903	-	C-O stretch C-H vibration in cellulose
794	-	-	-	-	C-O bond in cellulose/hemicellulose/lignin

3.4.2. SEM Images of CA, CA-KM, and CA/ALG Nanofibers

The average fiber diameter (n=100) for 15% CA nanofibers was 325 ± 138 nm as shown in Figure 10(a). If observed in the figure, there was an appearance of beads circled in red. The fiber distributions are also varied, ranging from 100 to 700 nm. The average fiber diameter of CA nanofibers is rather smaller than those reported in previous works (Gong et al., 2019; Sayyed et al., 2019). For 17% CA and CA-KM nanofibers, the average fiber diameters were 347 ± 101 nm and 418 ± 127 nm, as shown in Figure 10 (b-c). The fiber diameter distributions for both nanofibers appeared to be more uniform and oriented as compared to the distributions of 15% CA nanofibers. This explains that higher CA concentration in CA nanofibers improved the stability and nanofibers diameter uniformity for tissue engineering applications. The increment of diameters was noticeable when the concentration of the loaded Kaempferol (KM) increased compared to that of CA nanofibers alone. This increment of fiber diameter might be related to the fact that the blended solutions became more viscous as more KM was added. The increasing viscosity of the blended solutions might be attributed to intermolecular hydrogen bonding (O-H) between the OH group of ethanol and the OH group of KM. The possibility of multiple intermolecular hydrogen bonds between the solvent and KM might be increased when the concentration of KM in the blended solutions is raised. As a result of increasing kaempferol (KM) concentration, the viscosity of the blended CA polymer solution increased, which was evident during electrospinning and confirmed by visual changes in fiber morphology (i.e., increased fiber diameter). In the current study, electrospun nanofibers loaded with KM were observed to have larger diameters compared to neat CA nanofibers, suggesting reduced molecular mobility during jet elongation. This is consistent with our observation that highly viscous solutions are more challenging to stretch uniformly at the Taylor cone, leading to thicker fibers. Our findings align with those of Christensen et al. (2016) and Mohapatra et al. (2021), who reported that increased hydrogen bonding between drug and polymer (or solvent) can reduce molecular mobility, thus increasing solution viscosity. Since molecular mobility and viscosity are inversely related (Mohapatra et al., 2021), stronger KM–ethanol interactions in our blend likely contributed to higher resistance to flow. This directly influenced fiber formation and morphology. Similar results were reported by Tawwab et al. (2019), who observed thicker fibers as a consequence of increased viscosity due to solute interactions. Therefore, while previous studies provide a useful framework, our experimental results independently support the relationship between drug–polymer interactions, viscosity, and fiber morphology in the CA-KM nanofiber system.

This difference in fiber diameter is attributed to the solvent concentration and concentration of CA. The diameter of electrospun nanofibers is a critical factor for improving drug loading and controlling drug release. The higher drug loading efficiency of nanofibers is related to the higher surface area to mass ratio (Shahriar et al., 2019). The surface area and porosity of nanofibers increase as the diameter of the fiber decreases. Furthermore, nanofibers with small diameters tend to form more interconnected architectures (Liao et al., 2018). As a result, the molecular mobility, such as main chain rotation and displacement, was reduced. The reduced molecular mobility has a substantial impact on drug release rates. In brief, the molecular mobility of amorphous chains was reduced as the diameter of nanofibers decreased, resulting in decreased drug release from the nanofibers (Chung & Kwak, 2018).

The SEM images of the nanofibers' surfaces and cross section of alginate hydrogel are shown in Figure 10 (a-d). The scaffolds' morphology and structure generally seemed to be quite similar, with each scaffold exhibiting a sponge-like structure. However, the composite scaffolds' appearance differed based on the materials utilised, the concentration of polymers, and the way that each particular polymer layered with alginate solution (Turnbull et al., 2018). However, it was possible to clearly see the porosity structure of the scaffolds. The pore size might range from 200 to 300 depending on the composite scaffolds (Figure 10d) for alginate hydrogel. When employed as a tissue engineering scaffold, pores with these diameters are appropriate for allowing cells to penetrate biomaterials and transport nutrients and waste (Wsoo et al., 2021). The method used to create the scaffolds and the way the scaffolds' specific area was treated to freeze-drying, had an impact on the distribution of the pore size within the scaffold, especially on the freezing process and frozen solvent sublimation direction (Wsoo et al., 2021). Overall, the composite scaffolds' shape and structure mirrored the essential qualities that a biomaterial scaffold must have in order to be used in tissue engineering applications (Turnbull et al., 2018).

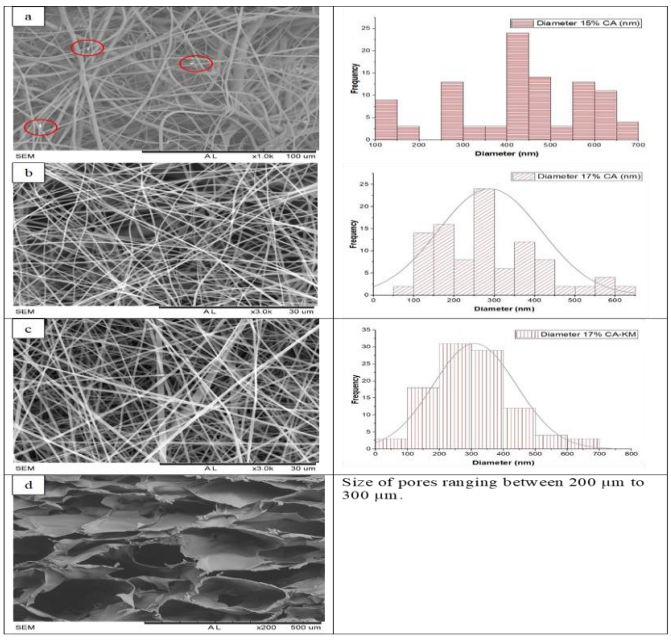

Figure 10. SEM images and fiber diameter distributions of (a) 15% CA nanofibers at a magnification of 1000x, (b) 17% CA nanofibers at a magnification of 3000x, (c) 17% CA-KM nanofibers at a magnification of 3000x, and (d) Cross section alginate solution layered on CA-KM nanofibers

3.4.3. Water Contact Angle

The surfacewetting of the CA nanofibrous membrane and KM-loaded CA nanofibers membrane was measured using water contact angle, and their results are illustrated in Figure 11 and summarized in Table 3. Based on Figure 11 (a, b), the 15% and 17% CA nanofiber membrane each had water contact angles of 108.00 ± 11.42° and 116.06 ± 9.00° respectively, indicating a hydrophobic nature (> 90) (Liu et al., 2021). As previously mentioned in the acetylation section, the surface wettability of CA nanofibers was affected and determined by the degree of substitution. The hydrophobicity of CA fibers increased as the degree of substitution increased because the hydroxyl group was replaced with an acetyl group (Mikaeili & Gouma, 2018). The surface wettability of the CA fibrous membrane was affected by the loaded KM (Figure 11c), which they have had 119.50 ± 4.88°, also indicating a hydrophobic surface (> 90). This can be explained by the presence of diphenylpropane in the flavonoid KM structure, which is responsible for its hydrophobicity (Ren et al., 2019). In Figure 11 (d), the water contact angle of the CA nanofiber that is layered with an alginate solution shows 0°, which indicates that it is highly hydrophilic. Alginate hydrogel is naturally hydrophilic and its porosity has further contributed to its hydrophilicity.

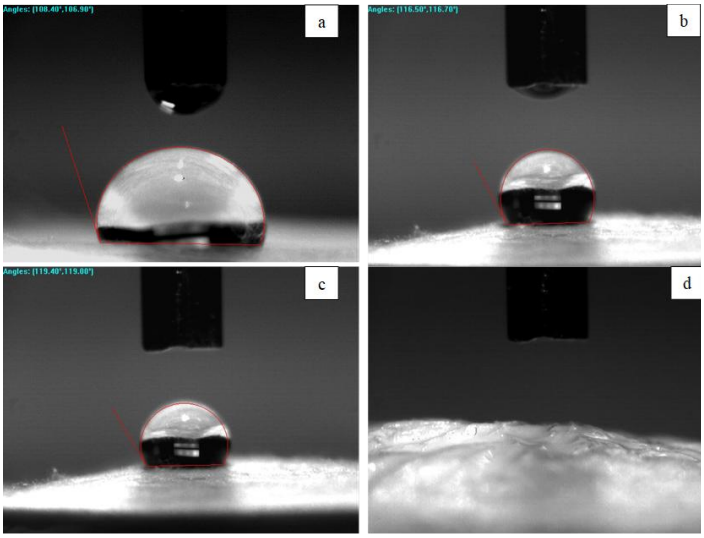

Figure 11. Water contact angle of (a) 15% CA nanofibers (b) 17% CA nanofibers (c) 17% CA-KM nanofibers (d) CA-KM/ALG

Table 3. Mean ± SD Water contact angle of various samples of CA and CA-KM/ALG

Samples	Mean ± SD Water contact angle in degree (°)
15% CA	108.00 ± 11.42
17% CA	116.06 ± 9.00
17% CA-KM	119.50 ± 4.88
17% CA-KM/ALG	0

3.4.4. Porosity of CA Nanofiber, CA-KM, CA/ALG, and CA-KM/ALG

In the context of wound healing and regeneration, nanofiber porosity is essential. It assists in controlling nutrient absorption, oxygen diffusion, and a site for cell adhesion (Prakash et al., 2021). Additionally, proper porosity is required for cell colonization and cell-to-cell interaction to restore, maintain, or regenerate skin tissue (Atila et al., 2016). Material with a porosity of nearly 90.00 ± 3.00% can be employed for tissue regeneration applications (Prakash et al., 2021). This is because such materials typically exhibit a rapid degradation rate and adequate water absorption, which facilitate and improve cell-material interactions and the formation of vascular networks (Ogueri & Laurencin, 2020). Based on Figure 12, CA/ALG scaffold showed the highest porosity value (94.00 ± 4.36%) compared to CA, CA-KM, and CA-KM/ALG. The porosity percentages for CA, CA-KM, and CA/ALG were 72.00 ± 6.24%, 68.33 ± 3.51%, and 91.30 ± 4.72% respectively. The decrease in porosity observed in KM-containing samples (CA-KM and CA-KM/ALG) compared to non-KM samples (CA and CA/ALG) may be attributed to the presence of KM, which contains four hydroxyl groups acting as hydrogen bond donor sites, as well as the C ring 4-oxo group that can participate in hydrogen bonding. In addition, the double bond (C2=C3 and C=O) in the C-ring of the KM molecule are key structural features that contribute to increased molecular stability (Trendafilova et al., 2021). These interactions may promote stronger intermolecular bonding within the nanofiber matrix, resulting in a more compact structure and reduced porosity. Furthermore, the incorporation of KM as a composite component may lead to the partial filling of nanofiber pores or voids, further decreasing overall porosity (Prakash et al., 2021).

Alginate hydrogels exhibit high porosity, which is highly advantageous for cell culture applications. Their porous structure allows cells to be seeded on the surface and penetrate into the hydrogel matrix. This characteristic facilitates the transport of small molecules and proteins, including growth factors (Ehterami et al., 2020). The water uptake properties of CA, CA-KM, CA/ALG, and CA-KM/ALG are influenced by several factors, including intermolecular interactions within the CA nanofibers, the incorporation of KM, the surface area of the samples, and the overall porosity of the CA nanofibers and alginate hydrogel (Ogeiri & Laurencin, 2020). Due to their porous nature, CA nanofibers and CA/ALG scaffolds exhibit higher porosity compared to drug-loaded fibers (Massana et al., 2021). Additionally, the relationship between water uptake and scanning electron microscopy (SEM) analysis of the fabricated nanofibers shows good agreement with the porosity results. The CA-KM/ALG nanofibers, with a porosity of 90.00 ± 5.29%, demonstrate strong potential for wound healing applications (Prakash et al., 2021). The scaffold porosity is suitable for permeation, allowing effective medium infiltration to support nutrient delivery and waste removal (Prakash et al., 2021).

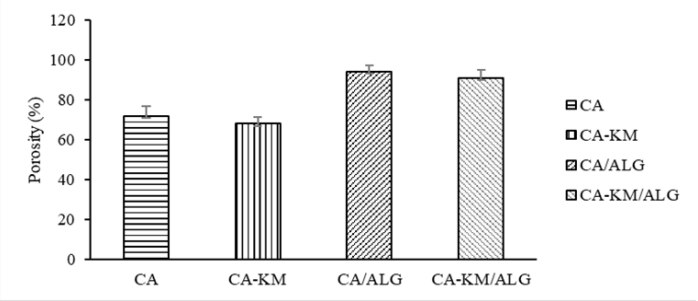

Figure 12 The porosity of each sample which are CA nanofibers, CA-KM nanofibers, CA/ALG, and CA-KM/ALG. Values are mean ± SD from three replicates

3.4.5. Degree of Water Uptake of CA, CA-KM, CA/ALG, and CA-KM/ALG

The water uptake characteristics of nanofibers are essential for regulating cell adhesion, infiltration, and nutrient transport (Prakash et al., 2021). The water uptake ratio of the scaffolds was evaluated to provide insight into their swelling behavior. The results, presented in Figure 13, show the water uptake percentages of four scaffolds (CA, CA-KM, CA/ALG, and CA-KM/ALG) over a period of 1–15 days. The results indicate that CA and CA-KM nanofibers swelled and reached a near-equilibrium state after approximately 13 days under atmospheric conditions. As shown in Figure 13, the water uptake ratios of these nanofibers (450–475%) are lower than those of alginate-layered nanofibers, namely CA/ALG and CA-KM/ALG (600–650%).

Although no significant difference was observed between the water uptake ratios of CA and CA-KM nanofibers, notable differences were evident between scaffolds with and without the alginate hydrogel layer. This suggests that the composition of the polymer nanofibers plays a critical role in determining water uptake capacity. However, this trend becomes less pronounced upon the incorporation of KM into the nanofibers. In general, hydrogels with lower water uptake ratios tend to exhibit higher cross-linking density (Prakash et al., 2021). Therefore, the equilibrium water uptake results indicate that alginate hydrogel-based scaffolds demonstrate superior water uptake capacity compared to nanofiber-only scaffolds. This behavior may be attributed to the effective cross-linking density within the alginate hydrogel network, as well as the interactions between alginate, nanofibers, gelatin interconnectivity, and KM incorporation (Ehterami et al., 2020).

CA nanofibers exhibited an initial water uptake ratio of 102%, which increased to 217% on Day 3 and continued to rise to approximately 450% by Day 11 before reaching equilibrium. Meanwhile, CA-KM nanofibers showed an initial water uptake of 98%, which increased to 198% on Day 3 and continued to rise until Day 11 before reaching equilibrium, following a trend similar to that of CA nanofibers. In contrast, CA/ALG and CA-KM/ALG scaffolds demonstrated significantly higher initial water uptake values of 210% and 220%, respectively. This behavior can be attributed to the high porosity and three-dimensional structure of the materials. Furthermore, hydrogen bonding interactions between KM and CA may enhance the intermolecular network within the matrix. Previous studies have reported that lower initial water uptake is observed when the drug interacts with or occupies the porous structure of drug-loaded nanofibers (Prakash et al., 2021). Consistent with this finding, both KM-incorporated scaffolds (CA-KM and CA-KM/ALG) exhibited slightly lower water uptake ratios compared to CA and CA/ALG scaffolds. Among all samples, CA/ALG exhibited the highest water uptake ratio, reaching a stable state by Day 7 (612%) and ultimately achieving equilibrium at Day 9 (650%).

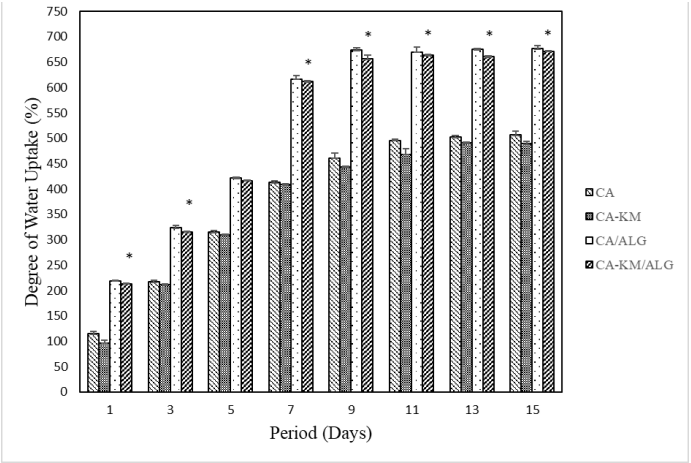

Figure 13 The degree of water uptake of each sample which are CA nanofibers, CA-KM nanofibers, CA/ALG, and CA-KM/ALG. Values are mean ± SD from three replicates with *$p < 0.05$ when is compared to CA nanofibers

3.4.6. Degree of Weight Loss of CA, CA-KM, CA/ALG, and CA-KM/ALG

The weight loss of materials or scaffolds typically begins when nanofibers come into contact with body fluids (Prakash et al., 2021). In this study, weight loss measurements were conducted concurrently with the water uptake analysis. The degradation behavior of the alginate hydrogel scaffolds was evaluated by calculating mass loss over the incubation period. As shown in Figure 14, CA/ALG degraded more rapidly and reached equilibrium by Day 9, with approximately 50% weight loss. In comparison, CA-KM nanofibers and CA-KM/ALG scaffolds exhibited slower degradation, both reaching equilibrium at Day 9 with weight losses of 45% and 23%, respectively. Meanwhile, CA nanofibers demonstrated the slowest degradation, reaching equilibrium at Day 11 with 28% weight loss. These results indicate that the incorporation of alginate hydrogel significantly increased the degradation rate of CA-KM, which may be attributed to reduced cross-linking density. The degradation of hydrogels facilitates cell infiltration into the scaffold matrix (Prakash et al., 2021). Notably, the CA/ALG nanofiber mat exhibited a higher weight loss rate at each time point compared to other samples, particularly between Day 9 and Day 15. This behavior can be explained by its high porosity (94%) and substantial water uptake (210%) during the initial period, which promote faster degradation. These characteristics also highlight the ability of alginate hydrogels to retain a significant amount of water within their structure without immediate dissolution, while still degrading over time. In

CA and CA-KM nanofibers, approximately 15% degradation was observed within 9 days. In contrast, CA/ALG and CA-KM/ALG scaffolds exhibited higher weight loss values of approximately 50% and 43%, respectively, by Day 9. This suggests a strong correlation between weight loss and water uptake, where increased swelling, reaching equilibrium around Day 9, and contributes to enhanced degradation behavior.

The incorporation of KM into the nanofiber mat may inhibit fluid-mediated degradation of the polymer at the wound site due to enhanced intermolecular interactions within the polymeric network (Prakash et al., 2021). As discussed in the water uptake analysis, a higher water uptake degree generally corresponds to weaker intermolecular bonding (Kai et al., 2017), which can accelerate material degradation. Fluid absorption is further promoted by the presence of hydrophilic functional groups, such as carboxyl and hydroxyl groups, leading to an increased weight loss of the scaffolds (Prakash et al., 2021). However, drug-loaded nanofibers (CA-KM and CA-KM/ALG) exhibited lower weight loss compared to non-drug-loaded nanofibers (CA and CA/ALG). This behavior is consistent with previous findings, where drug incorporation promotes additional polymeric interactions that reduce the availability of sites for fluid interaction, thereby limiting degradation (Prakash et al., 2021). Therefore, the in vitro weight loss results show a clear correlation with the water uptake data. Additionally, controlled degradation of the material is beneficial, as it supports the formation of a new extracellular matrix (ECM) at the wound site and provides space for cell differentiation, attachment, and proliferation (Kai et al., 2017).

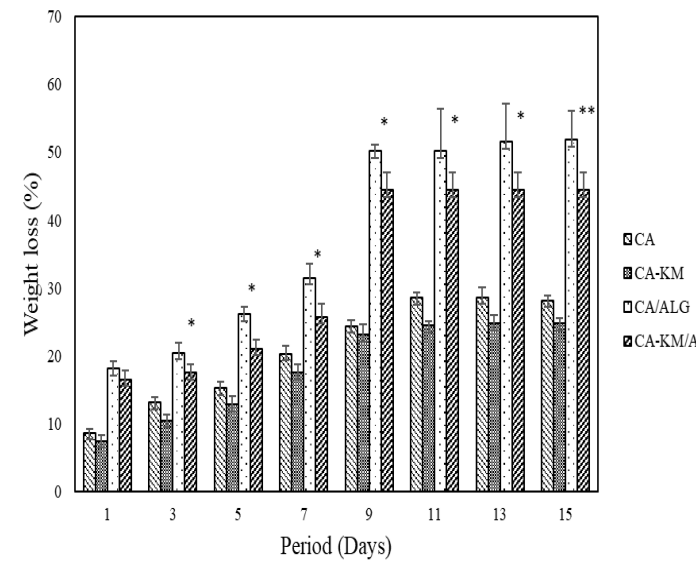

Figure 14. The weight loss percentage of each sample which are CA nanofibers, CA-KM nanofibers, CA/ALG, and CA-KM/ALG. Values are mean ± SD from three replicates with *p < 0.05

3.5. Evaluation of *in vitro* Cytotoxicity and Biocompatibility of CA, CA-KM, CA/ALG, and CA-KM/ALG

In this study, fibroblast cells were cultured *in vitro* on the CA, CA-KM, CA/ALG, and CA-KM/ALG to evaluate the biocompatibilities of the nanofiber's mats.

3.5.1. MTT Assay

The MTT result shows the cell viability of various concentrations of KM and the IC50 of KM on the fibroblast cell in Figure 15. This assay was done to determine the suitable KM concentration to be loaded into the CA nanofibers. Based on Figure 15 (a) and (b), KM at certain concentrations was shown to be biocompatible, which means that it is proven non-toxic and induces cell viability in both normo- and hyperglycemic microenvironments with both IC50 of 128 µg/mL and 147 µg/mL. Referring to the figures, both microenvironments were recorded to have the highest cell viability at 15.63 µg/mL when compared to the control group. MTT analysis showed that KM was non-toxic towards fibroblast cells and is compatible to be applied for wound healing applications. The cell viability above 80% is considered non-toxic when tested on fibroblast cells under ISO-10993-5 (Ullah et al., 2021).

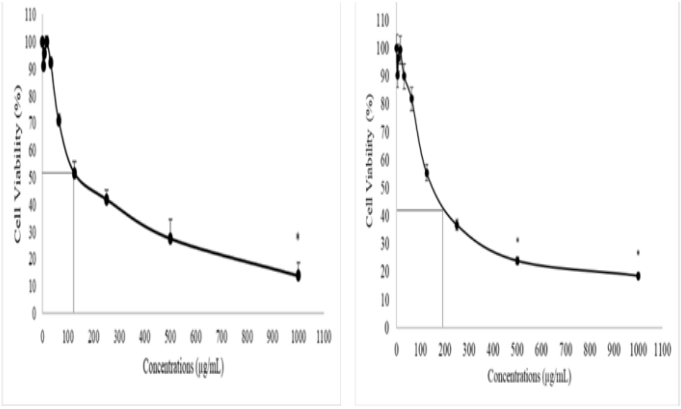

Figure 15 The effects of Kaempferol (KM) treatment on fibroblast cell under (a) normoglycemic and (b) hyperglycemic conditions with respective IC50. Values are mean ± SD from three replicates with *p < 0.05

3.5.2. Cell Attachment

The cell behaviours, namely attachment and proliferation, and cell morphology could be significantly dependent on the physicochemical properties, mechanical strength, and surface changes of nanofibers (Golizadeh et al., 2019). In cell attachment study, CCK-8 assay was performed to evaluate cell adhesion and proliferation on the scaffolds (Pan et al., 2019). Figures 16(a) and 16(b) show the cell attachment results on CA nanofibers after 4 hours of culture with fibroblast cells under normoglycemic and hyperglycemic conditions. The surface of CA nanofibers exhibited lower cell attachment compared to CA-KM nanofibers, which may be attributed to the presence of KM. KM imparts increased hydrophobicity, which can enhance the tendency for cellular adhesion (Ferrari et al., 2019). Meanwhile, CA/ALG and CA-KM/ALG scaffolds demonstrated higher cell attachment compared to CA and CA-KM nanofibers. This is likely due to the high porosity of the alginate hydrogel layer, which provides additional space and a favorable environment for cell growth (Sivaraj et al., 2021). This observation is consistent with previous studies reporting that membrane hydrophilicity significantly influences cell proliferation (Golizadeh et al., 2019; Lim et al., 2015).

Overall, an increasing trend in cell attachment was observed with the incorporation of KM, and this effect was further enhanced by the addition of the alginate hydrogel layer. It has also been reported that less uniform surface structures, often resulting from the presence of functional groups, can improve cell attachment, as cells generally exhibit better proliferation and bioactivity on rougher surfaces (Golizadeh et al., 2018). In this study, the alginate hydrogel layer further enhanced the scaffold surface by increasing the available surface area. This is supported by the observed results, indicating that the scaffolds are capable of supporting cell attachment and proliferation, making them suitable for tissue engineering applications. Additionally, previous studies have shown that modified nanofibers with improved hydrophilicity can promote consistent cell adhesion on the nanofiber surface (Lim et al., 2016).

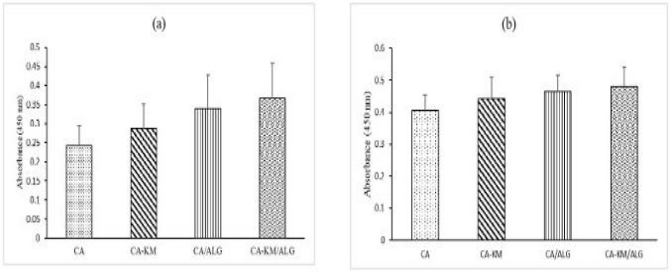

Figure 16 The fibroblast cell attachment under (a) normoglycemic and (b) hyperglycemic conditions. Values are mean ± SD from three replicates

3.5.3. Cell Proliferation

The proliferation of fibroblast cells on CA, CA-KM, CA/ALG, and CA-KM/ALG scaffolds under normoglycemic and hyperglycemic conditions was evaluated at 24, 48, and 72 hours using the CCK-8 assay. As shown in Figure 17(a), no significant differences in cell proliferation were observed among CA, CA-KM, CA/ALG, and CA-KM/ALG at 24 and 48 hours. However, at 72 hours, CA-KM/ALG scaffolds exhibited higher cell proliferation compared to CA nanofibers, indicating that CA-KM/ALG can enhance fibroblast proliferation over time. This improvement may be attributed to the formation of a biomimetic extracellular matrix (ECM)-like microstructure created by the embedded nanofibers within the hydrogel. Such ECM-like structures are known to promote cell–matrix interactions by providing additional binding sites for cell adhesion and proliferation (Xia et al., 2020). The incorporation of KM further contributed to enhanced cell proliferation, as observed in the comparison between CA and CA-KM nanofibers. CA-KM nanofibers showed higher cell proliferation, suggesting that both KM and the nanofiber-reinforced hydrogel system help maintain cell viability and promote proliferation. Furthermore, when co-cultured with fibroblast cells, no cytotoxic effects were observed from any of the samples, indicating that no harmful degradation products were released during incubation (Golizadeh et al., 2018). A similar trend was observed in CA/ALG and CA-KM/ALG scaffolds, where CA-KM/ALG demonstrated slightly higher cell proliferation than CA/ALG, although the difference was not statistically significant.

Meanwhile, in Figure 17(b), no significant differences in cell proliferation were observed among CA, CA-KM, CA/ALG, and CA-KM/ALG nanofibers. However, overall cell proliferation in the hyperglycemic microenvironment was lower across all time points compared to the normoglycemic condition. At 24 hours, cell proliferation showed comparable absorbance values among all samples, despite the overall lower levels under hyperglycemic conditions. At 48 hours, a slight increase in proliferation was observed; however, the values remained similar to those at 24 hours. Notably, CA-KM/ALG exhibited the highest absorbance among all samples at this time point. This behavior is consistent with the previously discussed findings under normoglycemic conditions, where KM incorporation and the nanofiber-reinforced hydrogel structure helped maintain cell viability and promote proliferation. Finally, at 72 hours, cell proliferation increased significantly compared to the earlier time points (24 and 48 hours), although it remained lower than that observed under normoglycemic conditions. This reduced proliferative activity may be attributed to slower fibroblast behavior in a hyperglycemic microenvironment due to elevated glucose levels, which can impair normal cellular function and proliferation.

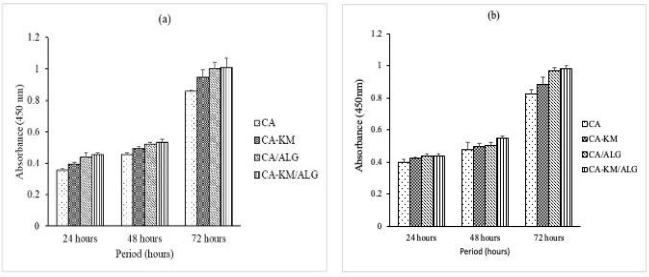

Figure 17 The fibroblast cell proliferation under (a) normoglycemic and (b) hyperglycemic conditions. Values are mean ± SD from three replicates

Integrating the findings of this study, it was observed that the incorporation of alginate solution into the nanofibers significantly improved hydrophilicity, cell adhesion properties, and wettability. In addition, the developed scaffolds enhanced cell–matrix interactions by providing an extracellular matrix (ECM)-mimicking microenvironment. Among all formulations, the CA-KM/ALG scaffold demonstrated the most promising performance and may serve as a potential substrate for tissue engineering applications in the treatment of chronic wound.

4. CONCLUSION

The main and interesting outcome of the present study is that a dual-layered potential chronic wound dressing from the electrospun CA/alginate nanofibers mat was fabricated successfully. The core of the electrospun consists of kaempferol-loaded CA nanofiber (CA-KM) and is layered with alginate solution. Based on the results and findings from this project, CA/ALG incorporated with KM

successfully delivered the KM to the fibroblast cell without causing cytotoxicity. All stated objectives have been addressed in the following point: cellulose acetate was obtained from a successfully extracted cellulose from rice husks. The characterisations from SEM and FTIR spectroscopy clearly depicted the microscopic structure and identified the chemical interactions of the samples in the respective extraction and acetylation processes. Prior to fabricating, CA and CA-KM nanofibers were dissolved in acetone/DMAC (2:1) and acetone/ethanol/DMAC (2:1:1) solvent systems and electrospun. The characterisations from SEM, FTIR, water contact angle, porosity, water uptake, and weight loss for both samples of CA and CA-KM nanofibers showed insignificant differences between the samples. The CA nanofibers surfaces were smooth, bead-free, and the nanofibers were randomly oriented with a uniform surface structure. Their morphology was not affected by the loading of KM. The fiber diameters from SEM were 347 ± 101 nm and 418 ± 127 nm, while FTIR analysis confirmed the loading of KM into the CA-KM nanofibers. The water contact angles for both samples were 108.00 ± 11.42° and 116.06 ± 9.00° and the porosity resulted in 72.00 ± 6.24% and 68.33 ± 3.51%. Water uptake recorded ranged from 450% to 475%, while weight loss was 28% and 24%. The alginate hydrogel layer was successfully crosslinked with the CA-KM nanofibers. The obtained results from SEM images showed uniform pore size distributions of ALG samples. For the degree of swelling and weight loss, both were observed to be influenced by KM and alginate hydrogel. The reduction of water uptake degree and weight loss were observed when KM was added but escalated with the addition of alginate hydrogel. In cytotoxicity, cell attachment and cell proliferation studies showed all samples (CA, CA-KM, CA/ALG, and CA-KM/ALG) were non-toxic to human fibroblast cells when the cells were attached after 4 hours of incubation and proliferated until 72 hours in each sample. As a result of the outcomes and convenience of the technologies outlined in this study, these developed nanofibers mats can be tested in vivo for wound healing activity on rat mode.

ACKNOWLEDGMENTS

This research was funded by Universiti Teknologi Malaysia through the Award Grant (5M006) and the Fundamental Research Grant (23H50).

AUTHOR CONTRIBUTIONS

Conceptualization, draft preparation, methodology, visualization, Aqilah M; draft preparation, Nasir. A.; reviewing, Bohari. S.P.; visualization, Salamun. N,; supervision, funding acquisition, Bohari. S.P. All authors have read and agreed to the published version of the manuscript

FUNDING

This research was funded by Universiti Teknologi

Malaysia with Grants no (R.J130000.7754.5M006) and

(Q.J130000.3854.23H50).

DATA AVAILABILITY

The processed data required to reproduce these findings cannot be shared at this time as the data also forms part of an ongoing study.

CODE AVAILABILITY

No code was involved in the work reported.

DECLARATIONS

Conflict of interest

Human and animal rights

No animal research was involved in the work reported.

Consent to participate

All authors have approved the manuscript and agree with submission.

Consent to publication

This work is original and has not been published elsewhere, or under consideration by another journal.

REFERENCES

[1] Achtel, C., & Heinze, T. (2016) 'Homogeneous acetylation of cellulose in the new solvent triethyloctylammonium chloride in combination with organic liquids', Macromolecular Chemistry and Physics, 217(18), 2041-2048.

[2] Adeli, H., Khorasani, M. T., & Parvazinia, M. (2019) 'Wound dressing based on electrospun PVA/chitosan/starch nanofibrous mats: Fabrication, antibacterial and cytocompatibility evaluation and in vitro healing assay', International journal of biological macromolecules, 122, 238-254.

[3] Afsharian, Y. P., & Rahimnejad, M. (2021) 'Bioactive electrospun scaffolds for wound healing applications: A comprehensive review', Polymer Testing, 93, 106952.

[4] Alam, W., Khan, H., Shah, M. A., Cauli, O., & Saso, L. (2020) 'Kaempferol as a dietary anti-inflammatory agent: current therapeutic standing', Molecules, 25(18), 4073.

[5] Ali, A., Mohebbullah, M., Shahid, M. A., Alam, S., Uddin, M. N., Miah, M. S., ... & Khan, M. S. (2021 'PVA-Nigella sativa nanofibrous mat: antibacterial efficacy and wound healing potentiality', The Journal of the Textile Institute, 112(10), 1611-1621.

[6] Ali, S., Khatri, Z., Oh, K. W., Kim, I. S., & Kim, S. H. (2014) 'Zein/cellulose acetate hybrid nanofibers: Electrospinning and characterization', Macromolecular Research, 22, 971-977.

[7] Alkhalidy, H., Moore, W., Wang, Y., Luo, J., McMillan, R. P., Zhen, W., ... & Liu, D. (2018) 'The flavonoid kaempferol ameliorates streptozotocin-induced diabetes by suppressing hepatic glucose production', Molecules, 23(9), 2338.

[8] Alven, S., Buyana, B., Feketshane, Z., & Aderibigbe, B. A. (2021) 'Electrospun nanofibers/nanofibrous scaffolds loaded with silver nanoparticles as effective antibacterial wound dressing materials', Pharmaceutics, 13(7), 964.

[9] Alves, J. A. A., Dos Santos, M. D. L., Morais, C. C., Ascheri, J. L. R., Signini, R., Dos Santos, D. M., ... & Ascheri, D. P. R. (2019) 'Sorghum straw: Pulping and bleaching process optimization and synthesis of cellulose acetate', International journal of biological macromolecules, 135, 877-886.

[10] Ambekar, R. S., & Kandasubramanian, B. (2019) 'Advancements in nanofibers for wound dressing: A review. European Polymer Journal, 117, 304-336.

[11] Angel, N., Guo, L., Yan, F., Wang, H., & Kong, L. (2020) 'Effect of processing parameters on the electrospinning of cellulose acetate studied by response surface methodology', Journal of Agriculture and Food Research, 2, 100015.

[12] Araujo, D., Castro, M. C. R., Figueiredo, A., Vilarinho, M., & Machado, A. (2020) 'Green synthesis of cellulose acetate from corncob: Physicochemical properties and assessment of environmental impacts', Journal of Cleaner Production, 260, 120865.

[13] Atila, D., Keskin, D., & Tezcaner, A. (2016) 'Crosslinked pullulan/cellulose acetate fibrous scaffolds for bone tissue engineering', Materials Science and Engineering: C, 69, 1103-1115.

[14] Bombin, A. D. J., Dunne, N. J., & McCarthy, H. O. (2020) 'Electrospinning of natural polymers for the production of nanofibres for wound healing applications', Materials Science and Engineering: C, 114, 110994.

[15] Brumberg, V., Astrelina, T., Malivanova, T., & Samoilov, A. (2021) 'Modern wound dressings: Hydrogel dressings', Biomedicines, 9(9), 1235.

[16] Candido, R. G., & Gonçalves, A. R. (2016) 'Synthesis of cellulose acetate and carboxymethylcellulose from sugarcane straw', Carbohydrate polymers, 152, 679-686.

[17] Castillo-Ortega, M. M., Montaño-Figueroa, A. G., Rodríguez-Félix, D. E., Munive, G. T., & Herrera-Franco, P. J. (2012) 'Amoxicillin embedded in cellulose acetate-poly (vinyl pyrrolidone) fibers prepared by coaxial electrospinning: Preparation and characterization', Materials Letters, 76, 250-254.

[18] Chang, Y. Y., Lai, C. H., Hsu, J. T., Tang, C. H., Liao, W. C., & Huang, H. L. (2012) 'Antibacterial properties and human gingival fibroblast cell compatibility of TiO 2/Ag compound coatings and ZnO films on titanium-based material', Clinical oral investigations, 16, 95-100.

[19] Cheah, W. K., Ooi, C. H., & Yeoh, F. Y. (2016) 'Rice husk and rice husk ash reutilization into nanoporous materials for adsorptive biomedical applications: A review', Open Material Sciences, 3(1).

[20] Cheah, W. K., Ooi, C. H., & Yeoh, F. Y. (2016) 'Rice husk and rice husk ash reutilization into nanoporous materials for adsorptive biomedical applications: A review', Open Material Sciences, 3(1).

[21] Chen, W., Chen, S., Morsi, Y., El-Hamshary, H., El-Newhy, M., Fan, C., & Mo, X. (2016) 'Superabsorbent 3D scaffold based on electrospun nanofibers for cartilage tissue engineering', ACS applied materials & interfaces, 8(37), 24415-24425.

[22] Chen, Y., Qiu, Y., Chen, W., & Wei, Q. (2020) 'Electrospun thymol-loaded porous cellulose acetate fibers with potential biomedical applications', Materials Science and Engineering: C, 109, 110536.

[23] Christensen, P. A., Attidekou, P. S., Egdell, R. G., Maneelok, S., & Manning, D. A. C. (2016) 'An in situ FTIR spectroscopic and thermogravimetric analysis study of the dehydration and dihydroxylation of SnO 2: the contribution of the (100),(110) and (111) facets', Physical Chemistry Chemical Physics, 18(33), 22990-22998.

[24] Chung, J., & Kwak, S. Y. (2018) 'Solvent-assisted heat treatment for enhanced chemical stability and mechanical strength of meta-aramid nanofibers', European Polymer Journal, 107, 46-53.

[25] Collazo-Bigliardi, S., Ortega-Toro, R., & Boix, A. C. (2018) 'Isolation and characterisation of microcrystalline cellulose and cellulose nanocrystals from coffee husk and comparative study with rice husk', Carbohydrate polymers, 191, 205-215.

[26] Colobatiu, L., Gavan, A., Potarniche, A. V., Rus, V., Diaconeasa, Z., Mocan, A., ... & Mihaiu, M. (2019) 'Evaluation of bioactive compounds-loaded chitosan films as a novel and potential diabetic wound dressing material', Reactive and Functional Polymers, 145, 104369.

[27] Das, A. M., Ali, A. A., & Hazarika, M. P. (2014) 'Synthesis and characterization of cellulose acetate from rice husk: Eco-friendly condition', Carbohydrate polymers, 112, 342-349.

[28] Dashtbani, R., & Afra, E. J. I. J. O. N. D. (2015) 'Producing cellulose nanofiber from cotton wastes by electrospinning method.

[29] Dhivya, S., Padma, V. V., & Santhini, E. (2015) 'Wound dressings–a review', BioMedicine, 5(4), 22.

[30] Ding, J., Zhang, J., Li, J., Li, D., Xiao, C., Xiao, H., ... & Chen, X. (2019) 'Electrospun polymer biomaterials', Progress in Polymer Science, 90, 1-34.

[31] Doostmohammadi, M., Forootanfar, H., & Ramakrishna, S. (2020) 'Regenerative medicine and drug delivery: Progress via electrospun biomaterials', Materials Science and Engineering: C, 109, 110521.

[32] Dumitriu, C., Voicu, S. I., Muhulet, A., Nechifor, G., Popescu, S., Ungureanu, C., ... & Pirvu, C. (2018) 'Production and characterization of cellulose acetate–titanium dioxide nanotubes membrane fraxiparinized through polydopamine for clinical applications', Carbohydrate polymers, 181, 215-223.

[33] Dunlop, M. J., Clemons, C., Reiner, R., Sabo, R., Agarwal, U. P., Bissessur, R., ... & Acharya, B. (2020) 'Towards the scalable isolation of cellulose nanocrystals from tunicates', Scientific reports, 10(1), 19090.

[34] Ehterami, A., Salehi, M., Farzamfar, S., Samadian, H., Vaez, A., Sahrapeyma, H., & Ghorbani, S. (2020) 'A promising wound dressing based on alginate hydrogels containing vitamin D3 cross-linked by calcium carbonate/d-glucono-δ-lactone', Biomedical Engineering Letters, 10, 309-319.

[35] Fahimirad, S., & Ajalloueian, F. (2019) 'Naturally-derived electrospun wound dressings for target delivery of bio-active agents', International journal of pharmaceutics, 566, 307-328.

[36] Fareez, I. M., Ibrahim, N. A., Wan Yaacob, W. M. H., Mamat Razali, N. A., Jasni, A. H., & Abdul Aziz, F. (2018) 'Characteristics of cellulose extracted from Josapine pineapple leaf fibre after alkali treatment followed by extensive bleaching', Cellulose, 25, 4407-4421.

[37] Ferrari, M., Cirisano, F., & Morán, M. C. (2019) 'Mammalian cell behavior on hydrophobic substrates: Influence of surface properties', Colloids and Interfaces, 3(2), 48.

[38] Gao, X., Guo, C., Hao, J., Zhao, Z., Long, H., & Li, M. (2020) 'Adsorption of heavy metal ions by sodium alginate based adsorbent-a review and new perspectives', International journal of biological macromolecules, 164, 4423-4434.

[39] Gizaw, M., Thompson, J., Faglie, A., Lee, S. Y., Neuenschwander, P., & Chou, S. F. (2018) 'Electrospun fibers as a dressing material for drug and biological agent delivery in wound healing applications', Bioengineering, 5(1), 9.

[40] Golizadeh, M., Karimi, A., Gandomi-Ravandi, S., Vossoughi, M., Khafaji, M., Joghataei, M. T., & Faghihi, F. (2019) 'Evaluation of cellular attachment and proliferation on different surface charged functional cellulose electrospun nanofibers', Carbohydrate polymers, 207, 796-805.

[41] Gong, Z., Du, Y., He, Y., Yang, A., Yang, Y., & Yu, D. (2019) 'The Influence of DMAc Ratio in Sheath Fluid on the Diameters of Medicated Cellulose Acetate Nanofibers', In International Conference on Biology, Chemistry and Medical Engineering (ICBCME 2019).

[42] Gopinath, V., Saravanan, S., Al-Maleki, A. R., Ramesh, M., & Vadivelu, J. (2018) 'A review of natural polysaccharides for drug delivery applications: Special focus on cellulose, starch and glycogen', Biomedicine & Pharmacotherapy, 107, 96-108.

[43] Graça, M. F., de Melo-Diogo, D., Correia, I. J., & Moreira, A. F. (2021) 'Electrospun asymmetric membranes as promising wound dressings: A review', Pharmaceutics, 13(2), 183.

[44] Gupta, P., Singh, B., Agrawal, A. K., & Maji, P. K. (2018) 'Low density and high strength nanofibrillated cellulose aerogel for thermal insulation application', Materials & Design, 158, 224-236.

[45] Haas D, Heinrich S, Greil P. Solvent control of cellulose acetate nanofibre felt structure produced by electrospinning. Journal of Materials Science. 2010;45:1299-1306

[46] Han, G., & Ceilley, R. (2017) 'Chronic wound healing: a review of current management and treatments', Advances in therapy, 34, 599-610.

[47] Hasanvand, E., & Rafe, A. (2018) 'Rheological and structural properties of rice bran protein-flaxseed (Linum usitatissimum L.) gum complex coacervates', Food Hydrocolloids, 83, 296-307.

[48] Huan, S., Bai, L., Liu, G., Cheng, W., & Han, G. (2015) 'Electrospun nanofibrous composites of polystyrene and cellulose nanocrystals: manufacture and characterization', Rsc Advances, 5(63), 50756-50766.

[49] Huhtamäki, T., Tian, X., Korhonen, J. T., & Ras, R. H. (2018) 'Surface-wetting characterization using contact-angle measurements', Nature protocols, 13(7), 1521-1538.

[50] Ilangovan, M., Guna, V., Prajwal, B., Jiang, Q., & Reddy, N. (2020) 'Extraction and characterisation of natural cellulose fibers from Kigelia africana', Carbohydrate polymers, 236, 115996.

[51] Jang, J., Seol, Y. J., Kim, H. J., Kundu, J., Kim, S. W., & Cho, D. W. (2014) 'Effects of alginate hydrogel cross-linking density on mechanical and biological behaviors for tissue engineering', Journal of the mechanical behavior of biomedical materials, 37, 69-77.

[52] Jatoi, A. W., Kim, I. S., & Ni, Q. Q. (2019) 'Cellulose acetate nanofibers embedded with AgNPs anchored TiO2 nanoparticles for long term excellent antibacterial applications', Carbohydrate polymers, 207, 640-649.

[53] Jeffcoate, W. J., Vileikyte, L., Boyko, E. J., Armstrong, D. G., & Boulton, A. J. (2018) 'Current challenges and opportunities in the prevention and management of diabetic foot ulcers', Diabetes care, 41(4), 645-652.

[54] Johar, N., Ahmad, I., & Dufresne, A. (2012) 'Extraction, preparation and characterization of cellulose fibres and nanocrystals from rice husk', Industrial Crops and Products, 37(1), 93-99.

[55] K Shukla, S., Dubey, C., Ashutosh Tiwari, G., & Bharadvaja, A. (2013) 'Preparation and characterization of cellulose derived from rice husk for drug delivery', Advanced Materials Letters, 4(9), 714-719.

[56] Kai, D., Zhang, K., Jiang, L., Wong, H. Z., Li, Z., Zhang, Z., & Loh, X. J. (2017) 'Sustainable and antioxidant lignin–polyester copolymers and nanofibers for potential healthcare applications', ACS Sustainable Chemistry & Engineering, 5(7), 6016-6025.

[57] Kalwar, K., Hu, L., Li, D. L., & Shan, D. (2018) 'AgNPs incorporated on deacetylated electrospun cellulose nanofibers and their effect on the antimicrobial activity', Polymers for Advanced Technologies, 29(1), 394-400.

[58] Kamal, T., Ahmad, I., Khan, S. B., & Asiri, A. M. (2017) 'Synthesis and catalytic properties of silver nanoparticles supported on porous cellulose acetate sheets and wet-spun fibers', Carbohydrate polymers, 157, 294-302.

[59] Kashyap, D., Sharma, A., Tuli, H. S., Sak, K., Punia, S., & Mukherjee, T. K. (2017) 'Kaempferol–A dietary anticancer molecule with multiple mechanisms of action: Recent trends and advancements', Journal of functional foods, 30, 203-219.

[60] Kaur, M., Sharma, P., & Kumari, S. (2021) 'State of art manufacturing and producing nanocellulose from agricultural waste: a review', Journal of Nanoscience and Nanotechnology, 21(6), 3394-3403.

[61] Kharaghani, D., Jo, Y. K., Khan, M. Q., Jeong, Y., Cha, H. J., & Kim, I. S. (2018) 'Electrospun antibacterial polyacrylonitrile nanofiber membranes functionalized with silver nanoparticles by a facile wetting method', European Polymer Journal, 108, 69-75.

[62] Khorasani, M. T., Joorabloo, A., Moghaddam, A., Shamsi, H., & MansooriMoghadam, Z. (2018) 'Incorporation of ZnO nanoparticles into heparinised polyvinyl alcohol/chitosan hydrogels for wound dressing application', International journal of biological macromolecules, 114, 1203-1215.

[63] Khoshnevisan, K., Maleki, H., Samadian, H., Shahsavari, S., Sarrafzadeh, M. H., Larijani, B., ... & Khorramizadeh, M. R. (2018) 'Cellulose acetate electrospun nanofibers for drug delivery systems: Applications and recent advances', Carbohydrate polymers, 198, 131-141.

[64] Konwarh, R., Karak, N., & Misra, M. (2013) 'Electrospun cellulose acetate nanofibers: the present status and gamut of biotechnological applications', Biotechnology advances, 31(4), 421-437.

[65] Kruer-Zerhusen, N., Cantero-Tubilla, B., & Wilson, D. B. (2018) 'Characterization of cellulose crystallinity after enzymatic treatment using Fourier transform infrared spectroscopy (FTIR)', Cellulose, 25, 37-48.

[66] Kurečič, M., Maver, T., Virant, N., Ojstršek, A., Gradišnik, L., Hribernik, S., ... & Kleinschek, K. S. (2018) 'A multifunctional electrospun and dual nano-carrier biobased system for simultaneous detection of pH in the wound bed and controlled release of benzocaine', Cellulose, 25, 7277-7297.

[67] Lai, W. F., Gui, D., Wong, M., Döring, A., Rogach, A. L., He, T., & Wong, W. T. (2021) 'A self-indicating cellulose-based gel with tunable performance for bioactive agent delivery', Journal of Drug Delivery Science and Technology, 63, 102428.

[68] Lamour, G., Hamraoui, A., Buvailo, A., Xing, Y., Keuleyan, S., Prakash, V., ... & Borguet, E. (2010) 'Contact angle measurements using a simplified experimental setup', Journal of chemical education, 87(12), 1403-1407.

[69] Landén, N. X., Li, D., & Ståhle, M. (2016) 'Transition from inflammation to proliferation: a critical step during wound healing', Cellular and Molecular Life Sciences, 73, 3861-3885.

[70] Latif, M. A., Ibrahim, F. W., Arshad, S. A., Hui, C. K., Jufri, N. F., & Hamid, A. (2019) 'Cytotoxicity, proliferation and migration rate assessments of human dermal fibroblast adult cells using zingiber zerumbet extract', Sains Malaysiana, 48(1), 121-127.

[71] Lavanya, D. K. P. K., Kulkarni, P. K., Dixit, M., Raavi, P. K., & Krishna, L. N. V. (2011) 'Sources of cellulose and their applications—A review', International Journal of Drug Formulation and Research, 2(6), 19-38.

[72] Li, Z., Wang, C., Li, Z., & Wang, C. (2013) 'Effects of working parameters on electrospinning', One-dimensional nanostructures: Electrospinning technique and unique nanofibers, 15-28.

[73] Liakos, I., Rizzello, L., Scurr, D. J., Pompa, P. P., Bayer, I. S., & Athanassiou, A. (2014) 'All-natural composite wound dressing films of essential oils encapsulated in sodium alginate with antimicrobial properties', International journal of pharmaceutics, 463(2), 137-145.

[74] Liao, Y., Loh, C. H., Tian, M., Wang, R., & Fane, A. G. (2018) 'Progress in electrospun polymeric nanofibrous membranes for water treatment: Fabrication, modification and applications', Progress in Polymer Science, 77, 69-94.

[75] Lima, D. S., Tenório-Neto, E. T., Lima-Tenório, M. K., Guilherme, M. R., Scariot, D. B., Nakamura, C. V., ... & Rubira, A. F. (2018) 'pH-responsive alginate-based hydrogels for protein delivery', Journal of Molecular Liquids, 262, 29-36.

[76] Liu, H., Ding, X., Zhou, G., Li, P., Wei, X., & Fan, Y. (2013) 'Electrospinning of nanofibers for tissue engineering applications', Journal of Nanomaterials, 2013, 3-3.

[77] Liu, T., Cai, C., Ma, R., Deng, Y., Tu, L., Fan, Y., & Lu, D. (2021) 'Super-hydrophobic cellulose nanofiber air filter with highly efficient filtration and humidity resistance', ACS applied materials & interfaces, 13(20), 24032-24041.

[78] Liu, Y., Zhou, S., Gao, Y., & Zhai, Y. (2019) 'Electrospun nanofibers as a wound dressing for treating diabetic foot ulcer', Asian Journal of Pharmaceutical Sciences, 14(2), 130-143.

[79] Long, Y. Z., Yan, X., Wang, X. X., Zhang, J., & Yu, M. (2019) 'Electrospinning: the setup and procedure', In Electrospinning: Nanofabrication and applications (pp. 21-52) 'William Andrew Publishing.

[80] Massana Roquero, D., McCorduck, B., Bollella, P., Smutok, O., Melman, A., & Katz, E. (2021) 'Biomolecule release from alginate composite hydrogels triggered by logically processed signals', ChemPhysChem, 22(19), 1967-1975.

[81] Maver, T., Kurečič, M., Pivec, T., Maver, U., Gradišnik, L., Gašparič, P., ... & Stana Kleinschek, K. (2020) 'Needleless electrospun carboxymethyl cellulose/polyethylene oxide mats with medicinal plant extracts for advanced wound care applications', Cellulose, 27, 4487-4508.

[82] Mele, E. (2016) 'Electrospinning of natural polymers for advanced wound care: towards responsive and adaptive dressings', Journal of Materials Chemistry B, 4(28), 4801-4812.

[83] Memic, A., Abdullah, T., Mohammed, H. S., Joshi Navare, K., Colombani, T., & Bencherif, S. A. (2019) 'Latest progress in electrospun nanofibers for wound healing applications', ACS Applied Bio Materials, 2(3), 952-969.

[84] Menon, M. P., Selvakumar, R., & Ramakrishna, S. (2017) 'Extraction and modification of cellulose nanofibers derived from biomass for environmental application', RSC advances, 7(68), 42750-42773.

[85] Mikaeili, F., & Gouma, P. I. (2018) 'Super water-repellent cellulose acetate mats', Scientific reports, 8(1), 12472.

[86] Mir, M., Ali, M. N., Barakullah, A., Gulzar, A., Arshad, M., Fatima, S., & Asad, M. (2018) 'Synthetic polymeric biomaterials for wound healing: a review', Progress in biomaterials, 7, 1-21.

[87] Mohapatra, T. K., Moharana, A. K., Swain, R. P., & Subudhi, B. B. (2021) 'Coamorphisation of acetyl salicylic acid and curcumin for enhancing dissolution, anti-inflammatory effect and minimizing gastro toxicity', Journal of Drug Delivery Science and Technology, 61, 102119.

[88] Moradkhannejhad, L., Abdouss, M., Nikfarjam, N., Mazinani, S., & Heydari, V. (2018) 'Electrospinning of zein/propolis nanofibers; antimicrobial properties and morphology investigation', Journal of Materials Science: Materials in Medicine, 29, 1-10.

[89] Moshfeghian, M., Azimi, H., Mahkam, M., Kalaee, M., Mazinani, S., & Mosafer, H. (2021) 'Effect of solution properties on electrospinning of polymer nanofibers: A study on fabrication of PVDF nanofibers by electrospinning in DMAC and (DMAC/acetone) solvents', Advances in Applied NanoBio-Technologies, 2(2), 53-58.

[90] Mousavi, S. M., Nejad, Z. M., Hashemi, S. A., Salari, M., Gholami, A., Ramakrishna, S., ... & Lai, C. W. (2021) 'Bioactive agent-loaded electrospun nanofiber membranes for accelerating healing process: A review', Membranes, 11(9), 702.

[91] Mutlu, G., Calamak, S., Ulubayram, K., & Guven, E. (2018) 'Curcumin-loaded electrospun PHBV nanofibers as potential wound-dressing material', Journal of Drug Delivery Science and Technology, 43, 185-193.

[92] Nasir, A., Razak, S. I. A., Adrus, N., Suan, C. L., Rahmat, Z., & Bohari, S. P. M. (2023). Fabrication and characterization of electrospun cellulose acetate nanofibers derived from rice husk for potential wound healing application. Cellulose, 30(5), 3153-3164.

[93] Negut, I., Dorcioman, G., & Grumezescu, V. (2020) 'Scaffolds for wound healing applications', Polymers, 12(9), 2010.

[94] Nguyen, T. D., Nguyen, T. T., Ly, K. L., Tran, A. H., Nguyen, T. T. N., Vo, M. T., ... & Nguyen, T. H. (2019) 'In vivo study of the antibacterial chitosan/polyvinyl alcohol loaded with silver nanoparticle hydrogel for wound healing applications', International Journal of Polymer Science, 2019.

[95] Ogueri, K. S., & Laurencin, C. T. (2020) 'Nanofiber technology for regenerative engineering', ACS nano, 14(8), 9347-9363.

[96] Onoja, E., & Wahab, R. A. (2019) 'Effect of glutaraldehyde concentration on catalytic efficacy of Candida rugosa lipase immobilized onto silica from oil palm leaves', Indonesian Journal of Chemistry, 19(4), 1043-1054.

[97] Opneja, A., Kapoor, S., & Stavrou, E. X. (2019) 'Contribution of platelets, the coagulation and fibrinolytic systems to cutaneous wound healing', Thrombosis research, 179, 56-63.

[98] Özay, Y., Güzel, S., Yumrutaş, Ö., Pehlivanoğlu, B., Erdoğdu, İ. H., Yildirim, Z., ... & Darcan, S. (2019) 'Wound healing effect of kaempferol in diabetic and nondiabetic rats', Journal of Surgical Research, 233, 284-296.

[99] Pan, S., Zhong, Y., Shan, Y., Liu, X., Xiao, Y., & Shi, H. (2019) 'Selection of the optimum 3D-printed pore and the surface modification techniques for tissue engineering tracheal scaffold in vivo reconstruction', Journal of Biomedical Materials Research Part A, 107(2), 360-370.

[100] Pang, C., Ibrahim, A., Bulstrode, N. W., & Ferretti, P. (2017) 'An overview of the therapeutic potential of regenerative medicine in cutaneous wound healing', International Wound Journal, 14(3), 450-459.

[101] Paschoal, G. B., Muller, C. M., Carvalho, G. M., Tischer, C. A., & Mali, S. (2015) 'Isolation and characterization of nanofibrillated cellulose from oat hulls', Química Nova, 38, 478-482.

[102] Phiriyawirut, M., & Phaechamud, T. (2012) 'Cellulose acetate electrospun fiber mats for controlled release of silymarin', Journal of Nanoscience and Nanotechnology, 12(1), 793-799.

[103] Pinheiro Bruni, G., dos Santos Acunha, T., de Oliveira, J. P., Martins Fonseca, L., Tavares da Silva, F., Martins Guimarães, V., & da Rosa Zavareze, E. (2020) 'Electrospun protein fibers loaded with yerba mate extract for bioactive release in food packaging', Journal of the Science of Food and Agriculture, 100(8), 3341-3350.

[104] Prakash, J., Venkataprasanna, K. S., Bharath, G., Banat, F., Niranjan, R., & Venkatasubbu, G. D. (2021) 'In-vitro evaluation of electrospun cellulose acetate nanofiber containing Graphene oxide/TiO2/Curcumin for wound healing application', Colloids and Surfaces A: Physicochemical and Engineering Aspects, 627, 127166.

[105] Rahim, K., Saleha, S., Zhu, X., Huo, L., Basit, A., & Franco, O. L. (2017) 'Bacterial contribution in chronicity of wounds', Microbial ecology, 73, 710-721.

[106] Ravikumar, R., Ganesh, M., Senthil, V., Ramesh, Y. V., Jakki, S. L., & Choi, E. Y. (2018) 'Tetrahydro curcumin loaded PCL-PEG electrospun transdermal nanofiber patch: Preparation, characterization, and in vitro diffusion evaluations', Journal of Drug Delivery Science and Technology, 44, 342-348.

[107] Ravikumar, R., Ganesh, M., Ubaidulla, U., Choi, E. Y., & Jang, H. T. (2017) 'Preparation, characterization, and in vitro diffusion study of nonwoven electrospun nanofiber of curcumin-loaded cellulose acetate phthalate polymer', Saudi Pharmaceutical Journal, 25(6), 921-926.

[108] Razak, S. I. A., Dahli, F. N., Wahab, I. F., Abdul Kadir, M. R., Muhamad, I. I., Yusof, A. H. M., & Adeli, H. (2016) 'A Conductive polylactic acid/polyaniline porous scaffold via freeze extraction for potential biomedical applications', Soft Materials, 14(2), 78-86.

[109] Rbihi, S., Laallam, L., Sajieddine, M., & Jouaiti, A. (2019) 'Characterization and thermal conductivity of cellulose based composite xerogels', Heliyon, 5(5).

[110] Ren, J., Lu, Y., Qian, Y., Chen, B., Wu, T., & Ji, G. (2019) 'Recent progress regarding kaempferol for the treatment of various diseases', Experimental and therapeutic medicine, 18(4), 2759-2776.

[111] Ren, J., Lu, Y., Qian, Y., Chen, B., Wu, T., & Ji, G. (2019) 'Recent progress regarding kaempferol for the treatment of various diseases', Experimental and therapeutic medicine, 18(4), 2759-2776.

[112] Rezk, A. I., Mousa, H. M., Lee, J., Park, C. H., & Kim, C. S. (2019) 'Composite PCL/HA/simvastatin electrospun nanofiber coating on biodegradable Mg alloy for orthopedic implant application', Journal of Coatings Technology and Research, 16, 477-489.

[113] Robles-García, M. Á., Del-Toro-Sánchez, C. L., Márquez-Ríos, E., Barrera-Rodríguez, A., Aguilar, J., Aguilar, J. A., ... & Rodríguez-Félix, F. (2018) 'Nanofibers of cellulose bagasse from Agave tequilana Weber var. azul by electrospinning: preparation and characterization', Carbohydrate polymers, 192, 69-74.

[114] Saghazadeh, S., Rinoldi, C., Schot, M., Kashaf, S. S., Sharifi, F., Jalilian, E., ... & Khademhosseini, A. (2018) 'Drug delivery systems and materials for wound healing applications', Advanced drug delivery reviews, 127, 138-166.

[115] Samadian, H., Zamiri, S., Ehterami, A., Farzamfar, S., Vaez, A., Khastar, H., ... & Salehi, M. (2020) 'Electrospun cellulose acetate/gelatin nanofibrous wound dressing containing berberine for diabetic foot ulcer healing: In vitro and in vivo studies', Scientific Reports, 10(1), 8312.

[116] Sankararamakrishnan, N., Shankhwar, A., & Chauhan, D. (2019) 'Mechanistic insights on immobilization and decontamination of hexavalent chromium onto nano MgS/FeS doped cellulose nanofibres', Chemosphere, 228, 390-397.

[117] Sarong, M. M., Orge, R. F., Eugenio, P. J. G., & Monserate, J. J. (2020) 'Utilization of rice husks into biochar and nanosilica: For clean energy, soil fertility and green nanotechnology', Int J Des Nat Ecodyn, 15(1), 97-102.

[118] Savencu, I., Iurian, S., Porfire, A., Bogdan, C., & Tomuță, I. (2021) 'Review of advances in polymeric wound dressing films', Reactive and Functional Polymers, 168, 105059.

[119] Sayyed, A. J., Deshmukh, N. A., & Pinjari, D. V. (2019) 'A critical review of manufacturing processes used in regenerated cellulosic fibres: viscose, cellulose acetate, cuprammonium, LiCl/DMAc, ionic liquids, and NMMO based lyocell', Cellulose, 26, 2913-2940.

[120] Seddiqi, H., Oliaei, E., Honarkar, H., Jin, J., Geonzon, L. C., Bacabac, R. G., & Klein-Nulend, J. (2021) 'Cellulose and its derivatives: Towards biomedical applications', Cellulose, 28(4), 1893-1931.

[121] Sen, C. K. (2021) 'Human wound and its burden: updated 2020 compendium of estimates', Advances in wound care, 10(5), 281-292.

[122] Sghaier, A. E. O. B., Chaabouni, Y., Msahli, S., & Sakli, F. (2012) 'Morphological and crystalline characterization of NaOH and NaOCl treated Agave americana L. fiber', Industrial Crops and Products, 36(1), 257-266.

[123] Shahriar, S. S., Mondal, J., Hasan, M. N., Revuri, V., Lee, D. Y., & Lee, Y. K. (2019) 'Electrospinning nanofibers for therapeutics delivery', Nanomaterials, 9(4), 532.

[124] Sharaf, S. S., El-Shafei, A. M., Refaie, R., Gibriel, A. A., & Abdel-Sattar, R. (2022) 'Antibacterial and wound healing properties of cellulose acetate electrospun nanofibers loaded with bioactive glass nanoparticles; in-vivo study', Cellulose, 29(8), 4565-4577.

[125] Shelke, N. B., Lee, P., Anderson, M., Mistry, N., Nagarale, R. K., Ma, X. M., ... & Kumbar, S. G. (2016) 'Neural tissue engineering: nanofiber-hydrogel based composite scaffolds', Polymers for Advanced Technologies, 27(1), 42-51.

[126] Singh, S., Young, A., & McNaught, C. E. (2017) 'The physiology of wound healing. Surgery (Oxford), 35(9), 473-477.

[127] Singh, T., Pattnaik, P., Aherwar, A., Ranakoti, L., Dogossy, G., & Lendvai, L. (2022) 'Optimal Design of Wood/Rice Husk-waste-Filled PLA Biocomposites Using Integrated CRITIC–MABAC-Based Decision-Making Algorithm', Polymers, 14(13), 2603.

[128] Sivaraj, D., Chen, K., Chattopadhyay, A., Henn, D., Wu, W., Noishiki, C., ... & Gurtner, G. C. (2021) 'Hydrogel scaffolds to deliver cell therapies for wound healing', Frontiers in bioengineering and biotechnology, 9, 660145.

[129] ŠTILET, P., & PLANINŠEK RUČIGAJ, T. A. N. J. A. (2016) 'Dressings for chronic wounds treatment', Acta medica Croatica: Časopis Akademije

medicinskih znanosti Hrvatske, 70(Suplement 1), 69-77.

[130] Stoyanova, N., Spasova, M., Manolova, N., Rashkov, I., Georgieva, A., & Toshkova, R. (2022) 'Quercetin-and Rutin-Containing Electrospun Cellulose Acetate and Polyethylene Glycol Fibers with Antioxidant and Anticancer Properties', Polymers, 14(24), 5380.

[131] Sultan, S., & Mathew, A. (2019) '3D printed nanocellulose scaffolds designed for biomedical applications', In ACS National Meeting & Exposition, Orlando, Florida, March 31-April 4, 2019.

[132] Sultana, N., & Zainal, A. (2016) 'Cellulose acetate electrospun nanofibrous membrane: fabrication, characterization, drug loading and antibacterial properties', Bulletin of Materials Science, 39, 337-343.

[133] Suwantong, O., Ruktanonchai, U., & Supaphol, P. (2010) 'In vitro biological evaluation of electrospun cellulose acetate fiber mats containing asiaticoside or curcumin', Journal of Biomedical Materials Research Part A, 94(4), 1216-1225.

[134] Tawwab, M. Y. A., Abdel-Hady, B. M., Rizk, R. A. E. M., & Shafaa, M. W. (2019) 'Effect of electrospinning parameters on the versatile production of polycaprolacton/gelatin nanofibre mats', Advances in Natural Sciences: Nanoscience and Nanotechnology, 10(2), 025009.

[135] Tian, S., Xie, H., Zhang, H., & Fu, S. (2021) 'Efficient separation of acetylated cellulose from eucalyptus and its enhancement on the mechanical strength of polylactic acid', International Journal of Biological Macromolecules, 191, 100-107.

[136] Torres-Martínez, E. J., Cornejo Bravo, J. M., Serrano Medina, A., Pérez González, G. L., & Villarreal Gómez, L. J. (2018) 'A summary of electrospun nanofibers as drug delivery system: Drugs loaded and biopolymers used as matrices', Current drug delivery, 15(10), 1360-1374.

[137] Trache, D., Tarchoun, A. F., Derradji, M., Hamidon, T. S., Masruchin, N., Brosse, N., & Hussin, M. H. (2020) 'Nanocellulose: from fundamentals to advanced applications', Frontiers in Chemistry, 8, 392.

[138] Tran, D. L., Le Thi, P., Thi, T. T. H., & Park, K. D. (2020) 'Novel enzymatically crosslinked chitosan hydrogels with free-radical-scavenging property and promoted cellular behaviors under hyperglycemia', Progress in Natural Science: Materials International, 30(5), 661-668.

[139] Trendafilova, I., Lazarova, H., Chimshirova, R., Trusheva, B., Koseva, N., & Popova, M. (2021) 'Novel kaempferol delivery systems based on Mg-containing MCM-41 mesoporous silicas', Journal of Solid State Chemistry, 301, 122323.

[140] Turnbull, G., Clarke, J., Picard, F., Riches, P., Jia, L., Han, F., ... & Shu, W. (2018) '3D bioactive composite scaffolds for bone tissue engineering', Bioactive materials, 3(3), 278-314.

[141] Ugheoke, I. B., & Mamat, O. (2012) 'A critical assessment and new research directions of rice husk silica processing methods and properties', Maejo international journal of science and technology, 6(3), 430.

[142] Ullah, A., Munir, S., Badshah, S. L., Khan, N., Ghani, L., Poulson, B. G., ... & Jaremko, M. (2020) 'Important flavonoids and their role as a therapeutic agent', Molecules, 25(22), 5243.

[143] Ullah, A., Ullah, S., Khan, M. Q., Hashmi, M., Nam, P. D., Kato, Y., ... & Kim, I. S. (2020) 'Manuka honey incorporated cellulose acetate nanofibrous mats: Fabrication and in vitro evaluation as a potential wound dressing', International journal of biological macromolecules, 155, 479-489.

[144] Vilchez, A., Acevedo, F., Cea, M., Seeger, M., & Navia, R. (2020) 'Applications of electrospun nanofibers with antioxidant properties: A review', Nanomaterials, 10(1), 175.

[145] Vivcharenko, V., & Przekora, A. (2021) 'Modifications of wound dressings with bioactive agents to achieve improved pro-healing properties', Applied Sciences, 11(9), 4114.

[146] Vowden, K., & Vowden, P. (2017) 'Wound dressings: principles and practice', Surgery (Oxford), 35(9), 489-494.

[147] Wang, M., Li, D., Li, J., Li, S., Chen, Z., Yu, D. G., ... & Guo, J. Z. (2020) 'Electrospun Janus zein–PVP nanofibers provide a two-stage controlled release of poorly water-soluble drugs', Materials & Design, 196, 109075.

[148] Wang, W., Liang, T., Bai, H., Dong, W., & Liu, X. (2018) 'All cellulose composites based on cellulose diacetate and nanofibrillated cellulose prepared by alkali treatment', Carbohydrate polymers, 179, 297-304.

[149] Wang, Z., Saleem, J., Barford, J. P., & McKay, G. (2020) 'Preparation and characterization of modified rice husks by biological delignification and acetylation for oil spill cleanup', Environmental Technology, 41(15), 1980-1991.

[150] Weller, C. D., Team, V., & Sussman, G. (2020) 'First-line interactive wound dressing update: A comprehensive review of the evidence', Frontiers in pharmacology, 11, 155.

[151] Wiegand, C., Abel, M., Hipler, U. C., & Elsner, P. (2019) 'Effect of non-adhering dressings on promotion of fibroblast proliferation and wound healing in vitro', Scientific Reports, 9(1), 4320.

[152] Wsoo, M. A., Shahir, S., Bohari, S. P. M., Nayan, N. H. M., & Abd Razak, S. I. (2020) 'A review on the properties of electrospun cellulose acetate and its application in drug delivery systems: A new perspective', Carbohydrate research, 491, 107978.

[153] Wsoo, M. A., Shahir, S., Bohari, S. P. M., Nayan, N. H. M., & Abd Razak, S. I. (2020) 'A review on the properties of electrospun cellulose acetate and its application in drug delivery systems: A new perspective', Carbohydrate research, 491, 107978.

[154] Wu, X. M., Branford-White, C. J., Zhu, L. M., Chatterton, N. P., & Yu, D. G. (2010) 'Ester prodrug-loaded electrospun cellulose acetate fiber mats as transdermal drug delivery systems', Journal of

Materials Science: Materials in Medicine, 21, 2403-2411.

[155] Wutticharoenmongkol, P., Hannirojram, P., & Nuthong, P. (2019) 'Gallic acid-loaded electrospun cellulose acetate nanofibers as potential wound dressing materials', Polymers for Advanced Technologies, 30(4), 1135-1147.

[156] Xie, X., Li, D., Chen, Y., Shen, Y., Yu, F., Wang, W., ... & Mo, X. (2021) 'Conjugate electrospun 3D gelatin nanofiber sponge for rapid hemostasis', Advanced healthcare materials, 10(20), 2100918.

[157] Yan, J., & Yu, D. G. (2012) 'Smoothening electrospinning and obtaining high-quality cellulose acetate nanofibers using a modified coaxial process', Journal of Materials Science, 47, 7138-7147.

[158] Yan, J., Liu, J., Sun, Y., Song, G., Ding, D., Fan, G., ... & Sun, L. (2021) 'Investigation on the preparation of rice straw-derived cellulose acetate and its spinnability for electrospinning', Polymers, 13(20), 3463.

[159] Ye, Y., Zhang, X., Deng, X., Hao, L., & Wang, W. (2019) 'Modification of alginate hydrogel films for delivering hydrophobic kaempferol', Journal of Nanomaterials, 2019, 1-8.

[160] Yoon, H. Y., Lee, E. G., Lee, H., Cho, I. J., Choi, Y. J., Sung, M. S., ... & Yoo, W. H. (2013) 'Kaempferol inhibits IL 1β induced proliferation of rheumatoid arthritis synovial fibroblasts and the production of COX 2, PGE2 and MMPs', International journal of molecular medicine, 32(4), 971-977.

[161] Yousefi, H., Azad, S., Mashkour, M., & Khazaeian, A. (2018) 'Cellulose nanofiber board', Carbohydrate polymers, 187, 133-139.

[162] Zhang, M., & Zhao, X. (2020) 'Alginate hydrogel dressings for advanced wound management', International Journal of Biological Macromolecules, 162, 1414-1428.

[163] Zhang, M., & Zhao, X. (2020) 'Alginate hydrogel dressings for advanced wound management', International Journal of Biological Macromolecules, 162, 1414-1428.

[164] Zhijiang, C., Cong, Z., Ping, X., Jie, G., & Kongyin, Z. (2018) 'Calcium alginate-coated electrospun polyhydroxybutyrate/carbon nanotubes composite nanofibers as nanofiltration membrane for dye removal', Journal of Materials Science, 53, 14801-14820.